

# Metrological characterisation of non-Gaussian entangled states of superconducting qubits

Kai Xu,<sup>1,\*</sup> Yu-Ran Zhang,<sup>2,\*</sup> Zheng-Hang Sun,<sup>1,\*</sup> Hekang Li,<sup>1</sup> Pengtao Song,<sup>1</sup> Zhongcheng Xiang,<sup>1</sup> Kaixuan Huang,<sup>1</sup> Hao Li,<sup>1</sup> Yun-Hao Shi,<sup>1</sup> Chi-Tong Chen,<sup>1</sup> Xiaohui Song,<sup>1</sup> Dongning Zheng,<sup>1</sup> Franco Nori,<sup>2,3,†</sup> H. Wang,<sup>4,‡</sup> and Heng Fan<sup>1,5,§</sup>

<sup>1</sup>*Institute of Physics, Chinese Academy of Sciences, Beijing 100190, China*

<sup>2</sup>*Theoretical Quantum Physics Laboratory, RIKEN Cluster for Pioneering Research, Wako-shi, Saitama 351-0198, Japan*

<sup>3</sup>*Physics Department, University of Michigan, Ann Arbor, Michigan 48109-1040, USA*

<sup>4</sup>*Interdisciplinary Centre for Quantum Information, State Key Laboratory of Modern Optical Instrumentation, and Zhejiang Province Key Laboratory of Quantum Technology and Device, Department of Physics, Zhejiang University, Hangzhou 310027, China*

<sup>5</sup>*CAS Centre for Excellence in Topological Quantum Computation, UCAS, Beijing 100190, China*

Multipartite entangled states are significant resources for both quantum information processing and quantum metrology [1]. In particular, non-Gaussian entangled states are predicted to achieve a higher sensitivity of precision measurements than Gaussian states [2]. On the basis of metrological sensitivity, the conventional linear Ramsey squeezing parameter (RSP) [3, 4] efficiently characterises the Gaussian entangled atomic states but fails for much wider classes of highly sensitive non-Gaussian states. These complex non-Gaussian entangled states can be classified by the nonlinear squeezing parameter (NLSP), as a generalisation of the RSP with respect to nonlinear observables [5], and identified via the Fisher information [6]. However, the NLSP has never been measured experimentally. Using a 19-qubit programmable superconducting processor, here we report the characterisation of multiparticle entangled states generated during its nonlinear dynamics. First, selecting 10 qubits, we measure the RSP and the NLSP by single-shot readouts of collective spin operators in several different directions. Then, by extracting the Fisher information of the time-evolved state of all 19 qubits, we observe a large metrological gain of  $9.89_{-0.29}^{+0.28}$  dB over the standard quantum limit [1], indicating a high level of multiparticle entanglement for quantum-enhanced phase sensitivity. Benefiting from high-fidelity full controls and addressable single-shot readouts, the superconducting processor with interconnected qubits provides an ideal platform for engineering and benchmarking non-Gaussian entangled states that are useful for quantum-enhanced metrology.

The ability to create and manipulate the entangled states of multiparticle quantum systems is crucial for advanced quantum technologies, including quantum metrology [1], quantum error correction [7], quantum communications [8, 9], quantum simulations [10], and fundamental tests of quantum theory [11]. A universal quantum computer is able to deterministically generate multiparticle entangled states with numerous sequences of single- and two-qubit operations. However, the conventional step-by-step method is very challenging to scale up and increases exposure to noise. Instead, parallel entangling operations, involving all-to-all connectivity, can efficiently create various types of entangled states, and have also been suggested to obtain polynomial or exponential speedups in some quantum algorithms and quantum simulation [12, 13]. Realised via the free evolution under a one-axis twisting (OAT) Hamiltonian, the parallel entangling operation first transforms the initial coherent spin state to squeezed spin states [4, 14] and then to non-Gaussian entangled states [2], including multicomponent atomic Schrödinger cat states and the GHZ state [15]. In the squeezed regime, squeezing of a collective spin, described by Gaussian statistics, represents the improvement of phase sensitivity to SU(2) rotations over the standard quantum limit [1, 4] and can be characterised by the Ramsey squeezing parameter (RSP)  $\xi_R^2$  [3]. In the over-squeezed regime, multipartite entanglement of the non-Gaussian spin states can be witnessed by extracting the Fisher information  $F$  [6], related to the phase sensitivity in Ramsey interferometry via the Cramér-Rao bound  $(\Delta\theta)^2 \geq 1/F$  [1, 4]. Furthermore, the non-Gaussian entangled states can

be classified by the nonlinear squeezing parameter (NLSP)  $\xi_{NL}^2$  [5], extending the concept of spin squeezing to nonlinear observables. Despite many achievements in generating linear spin squeezing (e.g., in Bose-Einstein condensates [16–21], atomic ensembles [22–33], and trapped ions [34]), the non-Gaussian entangled states, believed to perform higher-sensitive quantum phase estimation, quantum simulations [10] and classically intractable quantum algorithms, are attracting growing interests [35–38].

Here, we measure the NLSP using 10 interconnected superconducting qubits, which requires the capability of single-shot readouts of collective spin operators. Compared with the linear RSP and the Fisher information, our experiments help to analyse different classes of complicated non-Gaussian entangled states during the OAT evolution of the multi-qubit state. Moreover, by extracting the Fisher information, our experiments achieve a metrological gain,  $F/N = 9.89_{-0.29}^{+0.28}$  dB using  $N = 19$  qubits, which is larger than those obtained in many other experimental platforms with a much larger number of particles. Our work will stimulate interests in non-Gaussian entangled states of quantum many-body systems, with further applications in practical quantum metrology and quantum information processing.

In our experiments, 19 addressable transmon qubits ( $Q_j$ , with  $j$  varied from 1 to 19), capacitively coupled to a resonator bus R, are chosen to effectively engineer a OAT Hamiltonian, see Fig. 1a and refs. [15, 39]. By equally detuning selected qubits from the resonator by  $\Delta/2\pi \simeq -580$  MHz, the effec-

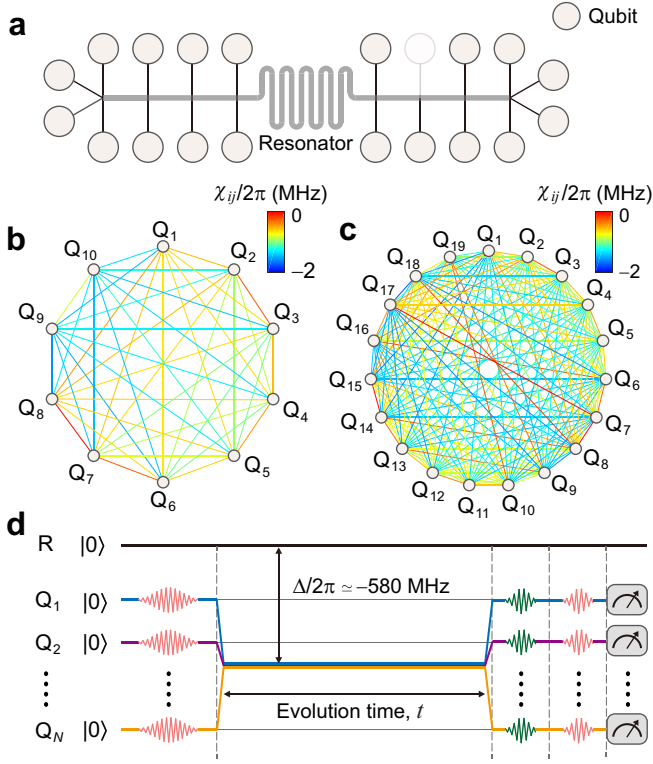


Fig. 1. **Superconducting quantum processor and experimental pulse sequence.** **a**, Simplified schematic of the superconducting quantum processor, showing 19 qubits interconnected by the central bus resonator R. **b**, **c**, Effective all-to-all coupling strengths,  $\chi_{ij}$ , for **(b)** selected 10 qubits and **(c)** all 19 qubits. **d**, Experimental waveform pulse sequence. Ten or nineteen qubits are initially prepared at  $|0\rangle$  at their idle points, and then transformed to  $|+\rangle$  by a collective  $Y_{\pi/2}$  gate. After the free evolution with a time  $t$ , when all qubits are equally detuned to the resonator R with  $\Delta/2\pi \approx -580$  MHz, all qubits at their idle points are measured in the same direction.

tive system Hamiltonian reads (we set  $\hbar = 1$ )

$$\hat{H} = \sum_{1 \leq i < j \leq N} \chi_{ij} (\hat{\sigma}_i^+ \hat{\sigma}_j^- + h.c.), \quad (1)$$

where  $\hat{\sigma}_j^+$  ( $\hat{\sigma}_j^-$ ) is the raising (lowering) operator of  $Q_j$ , and  $\chi_{ij}$  denotes the qubit-qubit coupling. As shown in Fig. 1b,c for choosing 10 qubits ( $Q_j$  with  $j = 1, 2, \dots, 10$ ) and all 19 qubits, respectively, the effect of unbalanced qubit-qubit couplings, caused by the few cross-talk couplings between neighbouring qubits, can be ignored, see also refs. [15, 39]. With  $N$  selected qubits initialised at their idle points as  $|00 \dots 0\rangle_N$ , we prepare these qubits in the state  $|++ \dots +\rangle_N$  via a  $Y_{\pi/2}$  pulse, and then detune them equally from the resonator R for the quench dynamics with a time  $t$  before the readouts in the same direction (see the experimental pulse sequence in Fig. 1d). Our  $N$ -qubit system can be described by a family of linear collective spin operators  $\hat{\mathbf{J}} \equiv (\hat{J}_x, \hat{J}_y, \hat{J}_z)$ , with  $\hat{J}_\beta \equiv \sum_{j=1}^N \hat{\sigma}_j^\beta / 2$ , and  $\hat{\sigma}_j^\beta$  being Pauli matrices for  $\beta = x, y, z$ . The Hamiltonian in Eq. (1) can be approximately expressed as a OAT one  $\hat{H} \simeq -\chi \hat{J}_z^2$ .

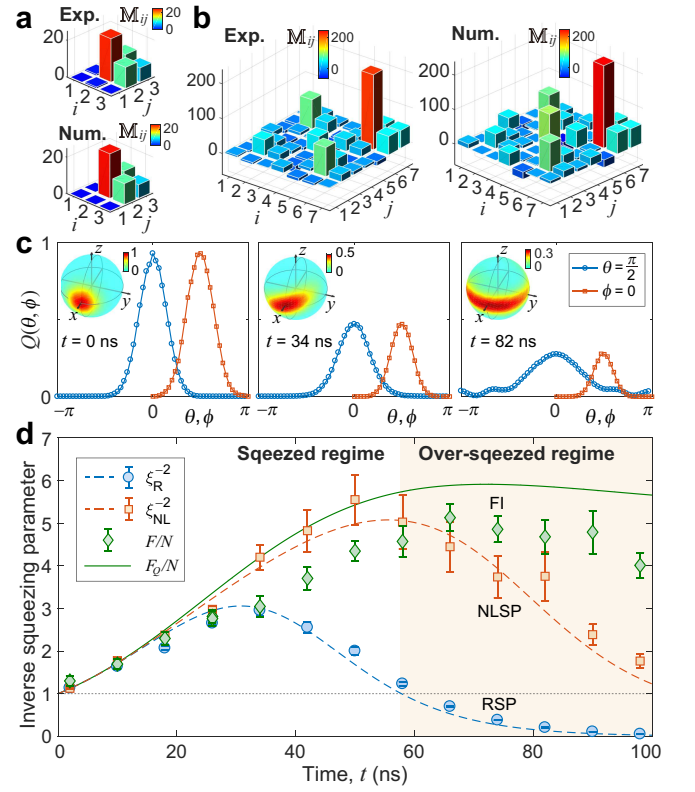


Fig. 2. **Linear Ramsey squeezing parameter versus nonlinear squeezing parameter for 10 superconducting qubits.** **a**, **b**, The measured matrices  $\mathbb{M}$  to optimise **(a)** the linear RSP at  $t = 34$  ns, and **(b)** the NLSP at  $t = 50$  ns, respectively, compared with the numerical simulations. **c**, Experimental data of the Husimi  $Q$  functions of the states,  $Q(\theta, \phi)$ , against  $\theta$  and  $\phi$  at specific times with the rotations along the  $x$ -axis to widen the equatorial distributions. At  $t = 0$  ns, 34 ns, and 82 ns, the  $Q(\theta, \phi)$  represent the spin-coherent state, the spin-squeezed state, and the non-Gaussian state, respectively. Insets: Experimentally measured  $Q(\theta, \phi)$  of the evolved states displayed in spherical polar. **d**, Time evolutions of the inverse linear RSP,  $\xi_R^{-2}$ , the inverse NLSP,  $\xi_{NL}^{-2}$ , with a family of operators  $\hat{\mathbf{S}}_{\text{exp}}$ , and the normalised Fisher information (FI),  $F/N$ , compared with the numerical simulations without decoherence (dashed curves). The green solid curve shows the numerical simulation of the normalised quantum Fisher information,  $F_Q/N = 4 \max_{\hat{n} \in \mathbb{R}^3} (\Delta_{\rho_t} \hat{J}_{\hat{n}})^2 / N$ , without decoherence, which is the largest normalised Fisher information over all possible measurements and linear generators. The error bars, indicating the standard deviations of the results, are calculated from 200,000 repetitive experimental runs in total (see Supplementary Information for details).

We need to estimate an unknown parameter  $\theta$ , imprinted on the time evolved state  $\rho_t$  at time  $t$  via unitary evolutions,  $\rho_t(\theta) = e^{-i\hat{J}_{\hat{n}}\theta} \rho_t e^{i\hat{J}_{\hat{n}}\theta}$ , with  $\hat{J}_{\hat{n}} \equiv \hat{n} \cdot \hat{\mathbf{J}}$  being a collective spin operator in the direction  $\hat{n} \in \mathbb{R}^3$ . For a family of  $D$  accessible operators  $\hat{\mathbf{S}} = (\hat{S}_1, \hat{S}_2, \dots, \hat{S}_D)$ , the parameter  $\theta$  is estimated from the measurement of the observable  $\hat{S}_{\hat{m}} = \hat{m} \cdot \hat{\mathbf{S}}$ , with  $\hat{m} \in \mathbb{R}^D$ , as a linear combination of accessible operators. Then, the optimal metrological squeezing parameter of  $\rho_t$  for

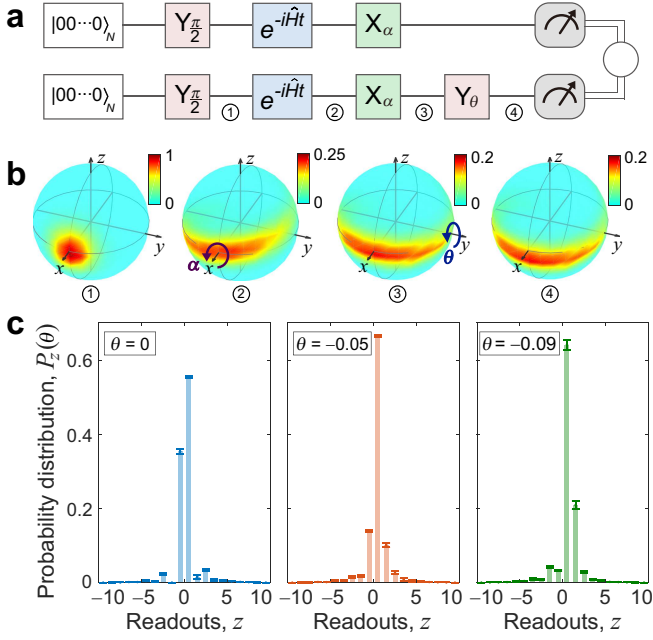


Fig. 3. **Experimental procedure for extracting the Fisher information for 19 superconducting qubits.** **a**, Schematic of the preparation, nonlinear evolution, optimisation rotation, measurement, and comparison of the readouts of two states, with and without the collective phase pulse  $Y_\theta$ ,  $\exp(-i\hat{J}_y\theta)$ , as in the Ramsey interferometer, for the extraction of the Fisher information. **b**, Experimental data of the  $Q$  functions,  $Q(\theta, \phi)$ , representing the states after ① the initial preparation, ② the nonlinear evolution with  $t = 48$  ns, ③ the collective optimisation rotation  $X_\alpha$ ,  $\exp(-i\hat{J}_x\alpha)$ , with  $\alpha = -0.288$  rad, and ④ the Ramsey pulse  $Y_\theta$ , respectively. **c**, The probability distributions  $P_z(\theta)$  of the measurement observable  $\hat{J}_z$  from the single-shot readout of each qubit, for  $\theta = 0$  rad,  $-0.05$  rad, and  $-0.09$  rad.

$\hat{S}$  can be written as [5]

$$\xi_{\text{opt}}^2[\rho_t, \hat{S}] = \min_{\hat{m} \in \mathbb{R}^D} \min_{\hat{n} \in \mathbb{R}^3} \frac{N(\Delta_{\rho_t} \hat{S} \hat{m})^2}{|(\hat{S} \hat{m}, \hat{J} \hat{n})_{\rho_t}|^2}, \quad (2)$$

where  $(\Delta_\rho \hat{O})^2 \equiv \langle \hat{O}^2 \rangle_\rho - \langle \hat{O} \rangle_\rho^2$  denotes the variance of the operator  $\hat{O}$  with respect to the state  $\rho$ . This parameter,  $\xi_{\text{opt}}^2[\rho_t, \hat{S}]$ , quantifies the achievable metrological sensitivity enhancement over the standard quantum limit. Its inverse  $\xi_{\text{opt}}^{-2}[\rho_t, \hat{S}] > \kappa$ , with  $1 \leq \kappa \leq (N-1)$ , reveals the multi-particle entanglement of at least  $(\kappa+1)$  qubits [40]. When the observables are limited to linear collective spin operators  $\hat{S}_{(1)} = \hat{J}$ , the  $\xi_{\text{opt}}^2[\rho_t, \hat{J}]$  reduces to the linear RSP  $\xi_{\text{R}}^2[\rho_t]$ . We can further define the NLSP  $\xi_{\text{NL}}^2[\rho_t]$  with an  $\hat{S}$  that includes not only linear but also nonlinear operators. For example, the second-order NLSP [5] corresponds to the  $D = 9$  linear and quadratic collective spin operators in different directions:  $\hat{S}_{(2)} = (\hat{J}_x, \hat{J}_y, \hat{J}_z, \hat{J}_x^2, \hat{J}_y^2, \hat{J}_z^2, \hat{J}_{xy}^2, \hat{J}_{yz}^2, \hat{J}_{zx}^2)$ , where  $\hat{J}_{\beta\gamma} \equiv (\hat{J}_\beta + \hat{J}_\gamma)/\sqrt{2}$ , with  $\beta, \gamma \in \{x, y, z\}$ .

With the method in ref. [5] to optimise measurement observables for quantum metrology, we first measure the linear RSP and the NLSP of  $N = 10$  qubits during the nonlinear

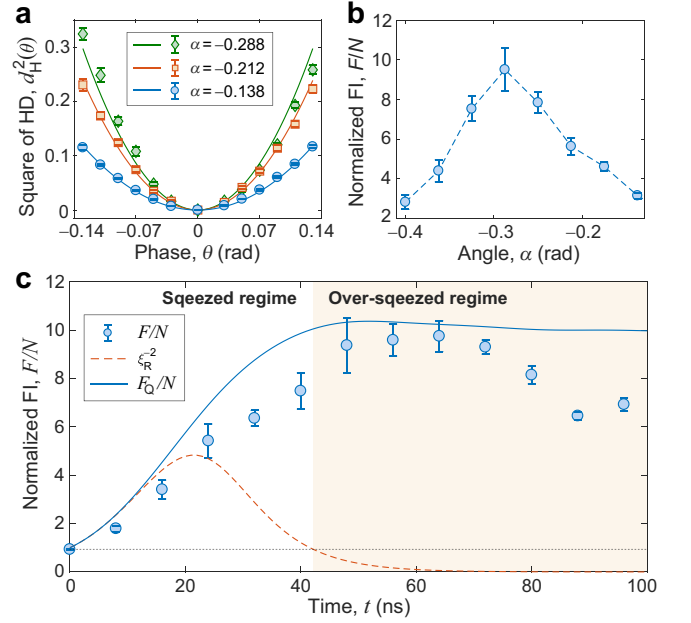


Fig. 4. **Quantum enhanced metrology with 19 superconducting qubits.** **a**, The squared Hellinger distance (HD) at  $t = 48$  ns versus the phase  $\theta$  in the Ramsey interferometer for different tomography angles  $\alpha = -0.288$  rad,  $-0.212$  rad, and  $-0.138$  rad (along the  $x$ -axis). The solid lines are for the quadratic curve fitting. **b**, The normalised Fisher information (FI),  $F/N$ , extracted from the squared Hellinger distance versus  $\alpha$ . The optimal angle at  $t = 48$  ns is obtained as  $\alpha_{\text{opt}} = -0.288$  rad. **c**, The time evolution of the normalised FI,  $F/N$ , is compared with the numerical simulations of the inverse RSP (red dashed curve),  $\xi_{\text{R}}^{-2}$ , and the normalised quantum Fisher information (blue solid curve),  $F_{\text{Q}}/N$ , without decoherence. The error bars, indicating the standard deviations of the results, are calculated from about 600,000 repetitive experimental runs in total (see Supplementary Information for details).

free evolution. The optimal metrological squeezing parameter can be obtained via searching the maximum eigenvalue  $\lambda_{\text{max}}$  of a  $3 \times 3$  matrix  $\tilde{\mathbb{M}}[\rho, \hat{S}]$  as [5]

$$\xi_{\text{opt}}^2[\rho_t, \hat{S}] = \frac{N}{\lambda_{\text{max}}(\tilde{\mathbb{M}}[\rho_t, \hat{S}])}, \quad (3)$$

where  $\tilde{\mathbb{M}}$  is the submatrix only containing the first three rows and columns of a  $D \times D$  matrix  $\mathbb{M}$ . The matrix  $\mathbb{M}$  reads

$$\mathbb{M}[\rho_t, \hat{S}] = \mathbb{C}^T[\rho_t, \hat{S}] \mathbb{V}^{-1}[\rho_t, \hat{S}] \mathbb{C}[\rho_t, \hat{S}], \quad (4)$$

where  $\mathbb{V}[\rho_t, \hat{S}]$  is the covariance matrix, with elements  $\mathbb{V}_{ij}[\rho_t, \hat{S}] = \langle \{\hat{S}_i, \hat{S}_j\} \rangle_{\rho_t} / 2 - \langle \hat{S}_i \rangle_{\rho_t} \langle \hat{S}_j \rangle_{\rho_t}$ , and  $\mathbb{C}[\rho_t, \hat{S}]$  is the real-valued skew-symmetric commutator matrix, with elements  $\mathbb{C}_{ij}[\rho_t, \hat{S}] = -i \langle [\hat{S}_i, \hat{S}_j] \rangle_{\rho_t}$ . For simplicity, we merely select seven collective spin operators (see Methods),  $\hat{S}_{\text{exp}} = (\hat{J}_x, \hat{J}_y, \hat{J}_z, \hat{J}_x^2, \hat{J}_y^2, \hat{J}_z^2, \hat{J}_{zx}^2)$ , and obtain the time evolution of the NLSP via measuring each element of  $\mathbb{V}[\rho_t, \hat{S}_{\text{exp}}]$  and  $\mathbb{C}[\rho_t, \hat{S}_{\text{exp}}]$  with simultaneous single-shot readouts of 10 qubits in different directions (see Supplementary Information

for more details). The RSP can be simply given by considering the submatrices  $\tilde{\mathbb{V}}$  and  $\tilde{\mathbb{C}}$ , only containing the first three rows and columns of  $\mathbb{V}$  and  $\mathbb{C}$ , respectively. At  $t = 34$  ns and 50 ns, the experimental data of matrices  $\mathbb{M}[\rho_t, \hat{\mathbf{J}}]$  and  $\mathbb{M}[\rho_t, \hat{\mathbf{S}}_{\text{exp}}]$  for the RSP and the NLSP, respectively, are compared with the numerical predictions in Fig. 2a,b. The time evolutions of the inverse RSP,  $\xi_{\text{R}}^{-2}$ , and the inverse NLSP,  $\xi_{\text{NL}}^{-2}$ , are shown in Fig. 2d, which are compared with the normalised Fisher information,  $F/N$ . Our results, verifying the hierarchical relationship,  $\xi_{\text{R}}^{-2} \leq \xi_{\text{NL}}^{-2}$ , demonstrate that the NLSP, generalising and improving the RSP with additional quadratic operators, helps to capture a larger set of metrologically useful entangled states. Especially, in the over-squeezed regime (e.g.,  $t = 82$  ns), the NLSP and the Fisher information identify the multiparticle entangled state with an obvious non-Gaussian distribution in phase space (Fig. 2c), which *cannot* be characterised by the linear RSP. Therefore, the NLSP, measured with single-shot readouts of collective spin operators, is efficient to capture the entanglement of the non-Gaussian state without the need of quantum state tomography.

Furthermore, the maximal Fisher information,  $F_{\text{opt}}$ , which quantifies the achievable metrological sensitivity with the optimal linear observable and linear generator, gives an upper bound to the inverse of the optimal metrological squeezing parameter  $F_{\text{opt}}/N \geq \xi_{\text{opt}}^{-2}[\rho_t, \hat{\mathbf{S}}]$  [5]. To demonstrate the metrological performance of our superconducting qubits, we experimentally detect the Fisher information by comparing the measurement statistics of the time evolved states  $\tilde{\rho}_t(0)$  and  $\tilde{\rho}_t(\theta)$  with and without a small rotation with the generator  $\hat{J}_y$  after the optimisation rotation along the  $x$ -axis (Fig. 3a). For a small  $\theta$  and sufficiently large number of experimental realisations, the Fisher information can be extracted as the coefficient of the quadratic term from a polynomial fit to the square of the Hellinger distance [2]: (Fig. 4a)

$$d_{\text{H}}^2(\theta) = \frac{F}{8}\theta^2 + \mathcal{O}(\theta^3), \quad (5)$$

where  $d_{\text{H}}^2(\theta) \equiv 1 - \sum_z \sqrt{P_z(0)P_z(\theta)}$ , and the sum is the Bhattacharyya coefficient with probability distributions  $P_z(0)$  and  $P_z(\theta)$  of the observable  $\hat{J}_z$  for states  $\tilde{\rho}_t(0)$  and  $\tilde{\rho}_t(\theta)$ , respectively (Fig. 3c). In Fig. 2d, we show with  $N = 10$  qubits that the Fisher information reveals larger multiparticle entanglement, though the RSP and the NLSP increase at long evolution times (e.g.,  $F/N \geq \xi_{\text{NL}}^{-2} \geq \xi_{\text{R}}^{-2}$ , with  $t \geq 66$  ns). The maximum normalised Fisher information,  $F/N = 5.13 \pm 0.32$  ( $7.10_{-0.28}^{+0.26}$  dB), is detected at  $t = 66$  ns for  $N = 10$  qubits. For  $N = 19$  qubits, we measure the Fisher information during the nonlinear time evolution as shown in Fig. 4c. At  $t = 64$  ns, we observe the maximum metrological gain  $F/N = 9.75 \pm 0.64$  ( $9.89_{-0.29}^{+0.28}$  dB), benefiting from the multiparticle entanglement of non-Gaussian states in the over-squeezed regime.

We have demonstrated the characterisation of multiparticle entangled states of superconducting qubits utilising different concepts of entanglement witnesses, including the RSP, the NLSP, and the Fisher information. With 19 qubits, we have

obtained a larger quantum metrological gain over the classical metrology than those obtained in many other platforms with much larger number of particles, representing the potential capability of showing quantum advantages in practical quantum metrology with interconnected superconducting qubits. Owing to the high-fidelity controls and individually addressable single-shot readouts of qubits with long decoherence times, our system is also promising for realising different quantum algorithms including two-axis-twisting spin squeezing [14] and variational quantum simulations [41].

**Acknowledgements** This work was supported by the National Key R&D Program of China (Grant Nos. 2016YFA0302104, 2016YFA0300600), the National Natural Science Foundation of China (Grant Nos. 11774406, 11934018, 11904393, 92065114), the Strategic Priority Research Program of Chinese Academy of Sciences (Grant No. XDB28000000), the NTT Research, the Army Research Office (ARO) (Grant No. W911NF-18-1-0358), the Japan Science and Technology Agency (JST) (via the Q-LEAP program and the CREST Grant No. JPMJCR1676), the Japan Society for the Promotion of Science (JSPS) (via the Postdoctoral Fellowship Grant No. P19326, the KAKENHI Grant Nos. JP19F19326, JP20H00134 and the JSPS-RFBR Grant No. JPISBP120194828), the Asian Office of Aerospace Research and Development (AOARD) (Grant No. FA2386-20-1-4069), and the Foundational Questions Institute Fund (FQXi) (Grant No. FQXi-IAF19-06).

**Author contributions** H.F., Y.-R.Z., and H.W. conceived the experiment. K.X. carried out the measurements. K.X. and Z.-H.S. analysed the experimental data. H.L. and D.Z. fabricated the device. Y.-R.Z., Z.-H.S. and K.X. designed the experiment and performed theoretical analysis. Y.-R.Z., K.X., Z.-H.S., F.N., H.W., and H.F. cowrote the manuscript. All authors contributed to the experimental setup, discussions of the results, and development of the manuscript.

**Competing interests** The authors declare no competing interests.

**Data availability** Data used in this work is available on reasonable request.

**Code availability** Code used in this work is available on reasonable request.

---

\* These authors contributed equally to this work.

† [fnori@riken.jp](mailto:fnori@riken.jp)

‡ [hhwang@zju.edu.cn](mailto:hhwang@zju.edu.cn)

§ [hfan@iphy.ac.cn](mailto:hfan@iphy.ac.cn)

- [1] V. Giovannetti, S. Lloyd, and L. Maccone, Advances in quantum metrology, *Nat. Photon.* **5**, 222 (2011).  
 [2] L. Pezzè, A. Smerzi, M. K. Oberthaler, R. Schmied, and P. Treut-

- lein, Quantum metrology with nonclassical states of atomic ensembles, *Rev. Mod. Phys.* **90**, 035005 (2018).
- [3] D. J. Wineland, J. J. Bollinger, W. M. Itano, and D. J. Heinzen, Squeezed atomic states and projection noise in spectroscopy, *Phys. Rev. A* **50**, 67 (1994).
- [4] J. Ma, X. G. Wang, C. P. Sun, and F. Nori, Quantum spin squeezing, *Phys. Rep.* **509**, 89 (2011).
- [5] M. Gessner, A. Smerzi, and L. Pezzè, Metrological nonlinear squeezing parameter, *Phys. Rev. Lett.* **122**, 090503 (2019).
- [6] S. L. Braunstein and C. M. Caves, Statistical distance and the geometry of quantum states, *Phys. Rev. Lett.* **72**, 3439 (1994).
- [7] E. T. Campbell, B. M. Terhal, and C. Vuillot, Roads towards fault-tolerant universal quantum computation, *Nature* **549**, 172 (2017).
- [8] Z. Zhao, Y.-A. Chen, A.-N. Zhang, T. Yang, H. J. Briegel, and J.-W. Pan, Experimental demonstration of five-photon entanglement and open-destination teleportation, *Nature* **430**, 54 (2004).
- [9] S. Wehner, D. Elkouss, and R. Hanson, Quantum internet: A vision for the road ahead, *Science* **362**, eaam9288 (2018).
- [10] I. M. Georgescu, S. Ashhab, and F. Nori, Quantum simulation, *Rev. Mod. Phys.* **86**, 153 (2014).
- [11] Z. Wang, H. Li, W. Feng, X. Song, C. Song, W. Liu, Q. Guo, X. Zhang, H. Dong, D. Zheng, H. Wang, and D.-W. Wang, Controllable switching between superradiant and subradiant states in a 10-qubit superconducting circuit, *Phys. Rev. Lett.* **124**, 013601 (2020).
- [12] Y. Lu, S. N. Zhang, K. Zhang, W. T. Chen, Y. C. Shen, J. L. Zhang, J.-N. Zhang, and K. Kim, Global entangling gates on arbitrary ion qubits, *Nature* **572**, 363 (2019).
- [13] C. Figgatt, A. Ostrander, N. M. Linke, K. A. Landsman, D. Zhu, D. Maslov, and C. Monroe, Parallel entangling operations on a universal ion-trap quantum computer, *Nature* **572**, 368 (2019).
- [14] M. Kitagawa and M. Ueda, Squeezed spin states, *Phys. Rev. A* **47**, 5138 (1993).
- [15] C. Song, K. Xu, H. K. Li, Y.-R. Zhang, X. Zhang, W. X. Liu, Q. J. Guo, Z. Wang, W. H. Ren, J. Hao, H. Feng, H. Fan, D. N. Zheng, D.-W. Wang, H. Wang, and S.-Y. Zhu, Generation of multicomponent atomic Schrödinger cat states of up to 20 qubits, *Science* **365**, 574 (2019).
- [16] C. Orzel, A. K. Tuchman, M. L. Fenselau, M. Yasuda, and M. A. Kasevich, Squeezed states in a Bose-Einstein condensate, *Science* **291**, 2386 (2001).
- [17] J. Estève, C. Gross, A. Weller, S. Giovanazzi, and M. K. Oberthaler, Squeezing and entanglement in a Bose-Einstein condensate, *Nature* **455**, 1216 (2008).
- [18] C. Gross, T. Zibold, E. Nicklas, J. Estève, and M. K. Oberthaler, Nonlinear atom interferometer surpasses classical precision limit, *Nature* **464**, 1165 (2010).
- [19] M. F. Riedel, P. Böhi, Y. Li, T. W. Hänsch, A. Sinatra, and P. Treutlein, Atom-chip-based generation of entanglement for quantum metrology, *Nature* **464**, 1170 (2010).
- [20] X.-Y. Luo, Y.-Q. Zou, L.-N. Wu, Q. Liu, M.-F. Han, M. K. Tey, and L. You, Deterministic entanglement generation from driving through quantum phase transitions, *Science* **355**, 620 (2017).
- [21] Y.-Q. Zou, L.-N. Wu, Q. Liu, X.-Y. Luo, S.-F. Guo, J.-H. Cao, M. K. Tey, and L. You, Beating the classical precision limit with spin-1 Dicke states of more than 10,000 atoms, *PNAS* **115**, 6381 (2018).
- [22] T. Fernholz, H. Krauter, K. Jensen, J. F. Sherson, A. S. Sørensen, and E. S. Polzik, Spin squeezing of atomic ensembles via nuclear-electronic spin entanglement, *Phys. Rev. Lett.* **101**, 073601 (2008).
- [23] S. Chaudhury, S. Merkel, T. Herr, A. Silberfarb, I. H. Deutsch, and P. S. Jessen, Quantum control of the hyperfine spin of a Cs atom ensemble, *Phys. Rev. Lett.* **99**, 163002 (2007).
- [24] J. Appel, P. J. Windpassinger, D. Oblak, U. B. Hoff, N. Kjærgaard, and E. S. Polzik, Mesoscopic atomic entanglement for precision measurements beyond the standard quantum limit, *PNAS* **106**, 10960 (2009).
- [25] T. Takano, S.-I.-R. Tanaka, R. Namiki, and Y. Takahashi, Manipulation of nonclassical atomic spin states, *Phys. Rev. Lett.* **104**, 013602 (2010).
- [26] I. D. Leroux, M. H. Schleier-Smith, and V. Vuletić, Implementation of cavity squeezing of a collective atomic spin, *Phys. Rev. Lett.* **104**, 073602 (2010).
- [27] M. H. Schleier-Smith, I. D. Leroux, and V. Vuletić, States of an ensemble of two-level atoms with reduced quantum uncertainty, *Phys. Rev. Lett.* **104**, 073604 (2010).
- [28] C. D. Hamley, C. S. Gerving, T. M. Hoang, E. M. Bookjans, and M. S. Chapman, Spin-nematic squeezed vacuum in a quantum gas, *Nat. Phys.* **8**, 305 (2012).
- [29] R. J. Sewell, M. Koschorreck, M. Napolitano, B. Dubost, N. Behbood, and M. W. Mitchell, Magnetic sensitivity beyond the projection noise limit by spin squeezing, *Phys. Rev. Lett.* **109**, 253605 (2012).
- [30] J. G. Bohnet, K. C. Cox, M. A. Norcia, J. M. Weiner, Z. Chen, and J. K. Thompson, Reduced spin measurement back-action for a phase sensitivity ten times beyond the standard quantum limit, *Nat. Photon.* **8**, 731 (2014).
- [31] R. McConnell, H. Zhang, J. Z. Hu, S. Čuk, and V. Vuletić, Entanglement with negative Wigner function of almost 3,000 atoms heralded by one photon, *Nature* **519**, 439 (2015).
- [32] O. Hosten, N. J. Engelsen, R. Krishnakumar, and M. A. Kasevich, Measurement noise 100 times lower than the quantum-projection limit using entangled atoms, *Nature* **529**, 505 (2016).
- [33] O. Hosten, R. Krishnakumar, N. J. Engelsen, and M. A. Kasevich, Quantum phase magnification, *Science* **352**, 1552 (2016).
- [34] J. G. Bohnet, B. C. Sawyer, J. W. Britton, M. L. Wall, A. M. Rey, M. Foss-Feig, and J. J. Bollinger, Quantum spin dynamics and entanglement generation with hundreds of trapped ions, *Science* **352**, 1297 (2016).
- [35] V. Parigi, A. Zavatta, M. Kim, and M. Bellini, Probing quantum commutation rules by addition and subtraction of single photons to/from a light field, *Science* **317**, 1890 (2007).
- [36] F. Haas, J. Volz, R. Gehr, J. Reichel, and J. Estève, Entangled states of more than 40 atoms in an optical fiber cavity, *Science* **344**, 180 (2014).
- [37] H. Strobel, W. Muessel, D. Linnemann, T. Zibold, D. B. Hume, L. Pezzè, A. Smerzi, and M. K. Oberthaler, Fisher information and entanglement of non-Gaussian spin states, *Science* **345**, 424 (2014).
- [38] U. L. Andersen, J. S. Neergaard-Nielsen, P. van Loock, and A. Furusawa, Hybrid discrete- and continuous-variable quantum information, *Nat. Phys.* **11**, 713 (2015).
- [39] K. Xu, Z.-H. Sun, W. X. Liu, Y.-R. Zhang, H. K. Li, H. Dong, W. H. Ren, P. F. Zhang, F. Nori, D. N. Zheng, H. Fan, and H. Wang, Probing dynamical phase transitions with a superconducting quantum simulator, *Sci. Adv.* **6**, eaba4935 (2020).
- [40] L. Pezzè and A. Smerzi, Entanglement, nonlinear dynamics, and the Heisenberg limit, *Phys. Rev. Lett.* **102**, 100401 (2009).
- [41] C. Kokail, C. Maier, R. van Bijnen, T. Brydges, M. K. Joshi, P. Jurcevic, C. A. Muschik, P. Silvi, R. Blatt, C. F. Roos, and P. Zoller, Self-verifying variational quantum simulation of lattice models, *Nature* **569**, 355 (2019).

## METHODS

### Experimental device

The device contains 20 superconducting qubits ( $q_j$  with  $j$  varied from 1 to 20), which are fully connected through a common resonator bus R. In our experiments, we use 19 of them, as one qubit ( $q_7$ ) suffers from a strong interaction with a two-level system near its working point. The qubit characteristics can be found in ref. [15], which is the same device used in this experiment. Extended Data Table I lists the latest device information for the participating qubits, obtained during this experiment. The full Hamiltonian of our quantum processor can be written as

$$\begin{aligned} \hat{H}_0 = & \omega_r \hat{a}^\dagger \hat{a} + \sum_{j=1}^{19} \omega_j \hat{\sigma}_j^+ \hat{\sigma}_j^- + \sum_{j=1}^{19} g_j (\hat{\sigma}_j^+ \hat{a} + \hat{\sigma}_j^- \hat{a}^\dagger) \\ & + \sum_{i<j} \chi_{ij}^c (\hat{\sigma}_i^+ \hat{\sigma}_j^- + \hat{\sigma}_j^+ \hat{\sigma}_i^-), \end{aligned} \quad (6)$$

where  $\omega_j/2\pi$  denotes the resonant frequency of  $q_j$  (individually tuneable from 3 GHz to 5.5 GHz). The frequency of the common resonator bus R, represented by  $\omega_r/2\pi$ , is fixed at about 5.51 GHz. Each qubit  $q_j$  is capacitively coupled to R, with magnitude,  $g_j/2\pi$ , listed in Extended Data Table I. Note that except for the dominant qubit-resonator interaction, there exist small direct couplings,  $\chi_{ij}^c/2\pi$ , between qubits in the system. In our experiments, by equally detuning the frequencies of all qubits far away from that of the resonator, we can realise the resonator-induced super-exchange interaction with a magnitude of  $g_i g_j / (2\pi \Delta)$  (with  $\Delta = \omega_i - \omega_r = \omega_j - \omega_r$ , and  $|\Delta| \gg g_i, g_j$ ) between *any* two qubits. The Hamiltonian can be further written as

$$\hat{H} = \sum_{i<j} (g_i g_j / \Delta + \chi_{ij}^c) (\hat{\sigma}_i^+ \hat{\sigma}_j^- + \hat{\sigma}_j^+ \hat{\sigma}_i^-). \quad (7)$$

The qubit-qubit coupling strengths

$$\chi_{ij} \equiv g_i g_j / \Delta + \chi_{ij}^c, \quad (8)$$

which can be experimentally estimated by the energy swapping process between  $q_i$  and  $q_j$  (see Supplementary materials of ref. [42]), are shown in Extended Data Fig. 1, with  $\Delta/2\pi \simeq -580$  MHz in this experiment.

For the 10-qubit experiment, we choose  $q_6, q_9, q_{10}, q_{11}, q_{12}, q_{13}, q_{14}, q_{17}, q_{18},$  and  $q_{20}$ . For the 19-qubit experiment, we choose 19 qubits except for  $q_7$ . In the main text, for convenience, the 19 qubits in order  $\{q_6, q_9, q_{10}, q_{11}, q_{12}, q_{13}, q_{14}, q_{17}, q_{18}, q_{20}, q_1, q_2, q_3, q_4, q_5, q_6, q_{15}, q_{16}, q_{19}\}$  are relabelled as  $\{Q_j\}$  with  $j = 1, 2, \dots, 19$ .

### Phase calibration

In our experiments, the nonlinear evolution  $\exp(-i\hat{H}t)$  is realised by equally detuning all the qubits from their idle

points,  $\omega_j/2\pi$ , to the interacting point,  $\omega_I/2\pi$ , by applying a rectangular pulse to each qubit. This operation will accumulate some dynamical phase, which needs to be cancelled via applying rotation pulses after the rectangular pulses. In theory, the dynamical phase can be estimated as  $2\pi\delta f \times t$ , where  $\delta f = (\omega_j - \omega_I)/2\pi$ . However, the imperfections of rectangular pulses, such as the imperfect rising and falling edges, will cause an additional phase shift from the theoretical calculations, which also needs to be experimentally calibrated. Extended Data Figure 2 shows the pulse sequence and the results of our phase calibration method, taking  $q_1$  as an example.  $q_1$  is tuned to the interacting point, while other qubits are arranged at their frequency points  $\omega_j^o/2\pi$  far away from  $\omega_I/2\pi$ . To minimise the Z-crosstalk effects of other qubits to  $q_1$  when being tuned away,  $\omega_j^o/2\pi$  are selected to have an equal Z-crosstalk effect on  $q_1$ , compared to the case when all qubits are tuned to  $\omega_I/2\pi$ , as can be estimated by the measured Z-crosstalk matrix  $M_Z$ . We monitor the  $|1\rangle$  state probability  $P(\phi, t)$  as a function of both the time  $t$  and the phase difference  $(\phi - 2\pi\delta f \times t)$ . For each time  $t$ , we perform a cosine fit to  $P(\phi, t)$  as a function of  $\phi$  to extract the phase shift  $\phi_+$ , caused by the imperfect rectangular pulses. To further reduce the Z-crosstalk effects and the ac-stark shift effects due to imperfect decoupling of other qubits to  $q_1$  when being tuned away, we perform this calibration process again with a little difference. The frequencies of other qubits are arranged at  $(2\omega_I - \omega_j^o)/2\pi$ , a symmetric position relative to  $\omega_I/2\pi$ . Again, we obtain the phase shift  $\phi_-$ . The final phase shift, used to cancel the dynamical phase, is  $(\phi_+ + \phi_-)/2$ , as shown by the red curves in Extended Data Fig. 2c.

### Efficient detection of second-order nonlinear squeezing parameter with seven operators

In our experiments, to obtain the nonlinear squeezing parameter, we select seven collective spin operators,

$$\hat{\mathbf{S}}_{\text{exp}} = (\hat{J}_x, \hat{J}_y, \hat{J}_z, \hat{J}_x^2, \hat{J}_y^2, \hat{J}_{xy}^2, \hat{J}_{yz}^2), \quad (9)$$

instead of the full family of the collective spin operators

$$\hat{\mathbf{S}}_{(2)} = (\hat{J}_x, \hat{J}_y, \hat{J}_z, \hat{J}_x^2, \hat{J}_y^2, \hat{J}_z^2, \hat{J}_{xy}^2, \hat{J}_{yz}^2, \hat{J}_{zx}^2), \quad (10)$$

for the second-order squeezing parameter [5]. As shown in Fig. 2d in the main text, we monitor the evolution of the nonlinear squeezing parameter via measuring each element of  $\mathbb{V}[\rho_t, \hat{\mathbf{S}}_{\text{exp}}]$  and  $\mathbb{C}[\rho_t, \hat{\mathbf{S}}_{\text{exp}}]$  (submatrices of  $\mathbb{V}[\rho_t, \hat{\mathbf{S}}_{(2)}]$  and  $\mathbb{C}[\rho_t, \hat{\mathbf{S}}_{(2)}]$ ) with simultaneous single-shot readouts of 10 qubits in different directions (see Supplementary Information). The numerical simulations of the inverse nonlinear squeezing parameters,  $\xi_{\text{NL}}^{-2}[\rho_t, \hat{\mathbf{S}}_{(2)}]$  and  $\xi_{\text{NL}}^{-2}[\rho_t, \hat{\mathbf{S}}_{\text{exp}}]$  with respect to  $\hat{\mathbf{S}}_{(2)}$  and  $\hat{\mathbf{S}}_{\text{exp}}$ , respectively, are compared in Extended Data Fig. 3. It is shown that the nonlinear squeezing parameter  $\xi_{\text{NL}}^{-2}[\rho_t, \hat{\mathbf{S}}_{\text{exp}}]$  with 7 selected collective spin operators is very close to the second-order nonlinear squeezing parameter  $\xi_{\text{NL}}^2[\rho_t, \hat{\mathbf{S}}_{\text{exp}}]$  for  $t \lesssim 76$  ns, and moreover, its minimum value

is close to that of the  $\xi_{\text{NL}}^2[\rho_t, \hat{\mathbf{S}}_{(2)}]$ . Therefore, when choosing these 7 collective spin operators, we can efficiently detect the second-order nonlinear squeezing parameter with fewer observables to be measured. At  $t = 2$  ns, 34 ns, and 50 ns, the experimental results of matrices  $\mathbb{C}[\rho_t, \hat{\mathbf{S}}_{\text{exp}}]$ ,  $\mathbb{V}[\rho_t, \hat{\mathbf{S}}_{\text{exp}}]$ , and  $\mathbb{M}[\rho_t, \hat{\mathbf{S}}_{\text{exp}}]$  are compared with numerical simulations in Extended Data Figs. 4, 5, and 6, respectively.

In addition, the method to optimise the squeezing parameter, based on searching for the largest eigenvalue of the matrix  $\mathbb{M}$  [5], requires a large number of trials of single-shot readouts for 19 observables (see Supplementary Information) to obtain a reliable value of the second-order squeezing parameter. Thus, choosing 7 collective spin operators instead of 9 operators in our experiments can significantly reduce the number of readouts, and almost detect the large sensitivity enhancement for quantum metrology, which is characterised by the second-order nonlinear squeezing parameter with 9 operators.

### Numerical details

Numerical computations are performed using the QUTIP [43, 44] (the quantum toolbox in PYTHON) and NUMPY. The time evolutions of the system with a Hamiltonian [Eq. (1)

in the main text] are numerically simulated using QUTIP's master equation solver `mesolve`, where the parameters in Extended Data Fig. 1 are used. Because the evolution time is much shorter than the qubits' energy relaxation time and dephasing time  $t \ll T_1, T_2$ , we neglect the effect of decoherence in simulations.

---

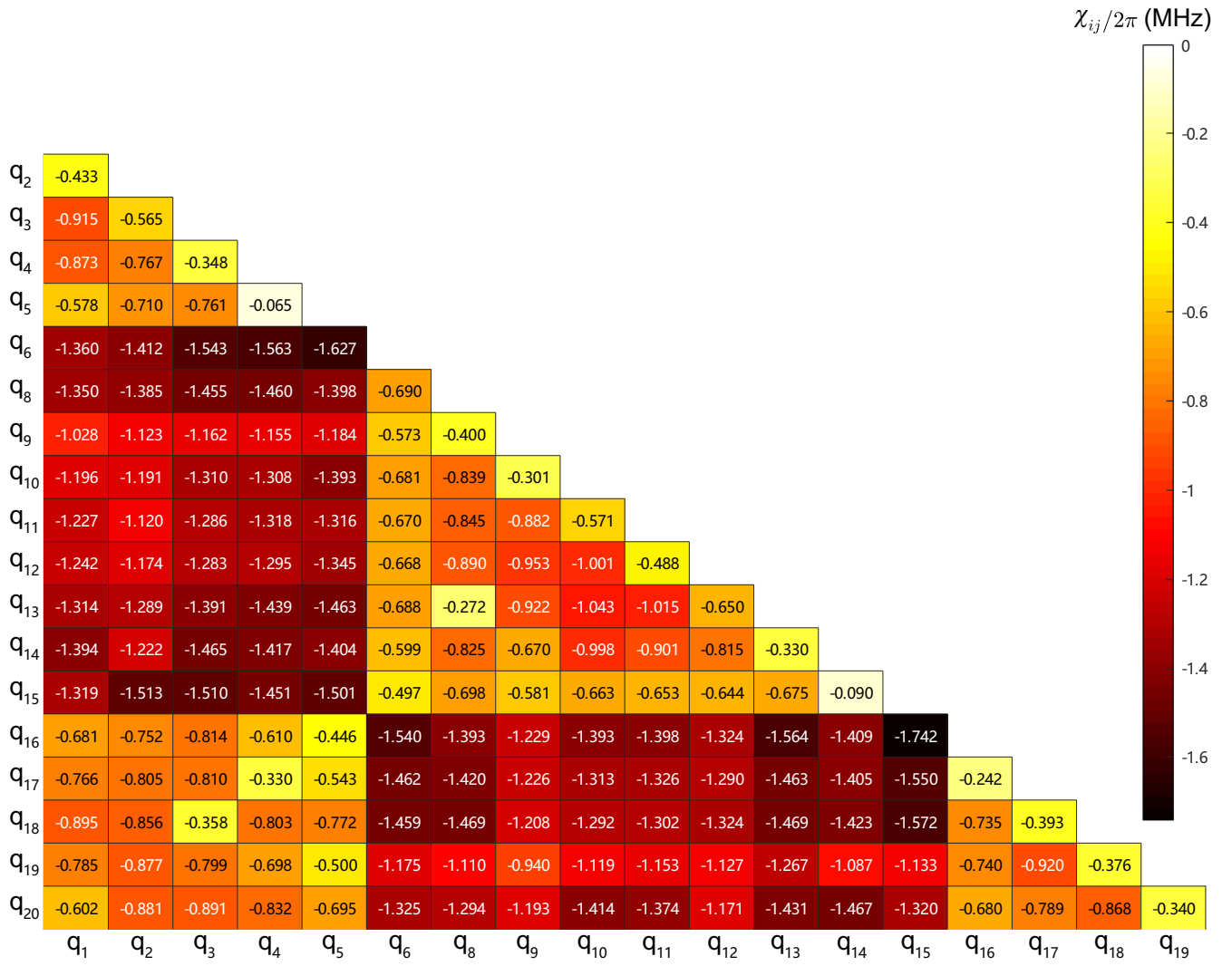
\* These authors contributed equally to this work.

† [fnori@riken.jp](mailto:fnori@riken.jp)

‡ [hhwang@zju.edu.cn](mailto:hhwang@zju.edu.cn)

§ [hfan@iphy.ac.cn](mailto:hfan@iphy.ac.cn)

- [42] C. Song, K. Xu, W. X. Liu, C. P. Yang, S. B. Zheng, H. Deng, Q. W. Xie, K. Q. Huang, Q. J. Guo, L. B. Zhang, P. F. Zhang, D. Xu, D. N. Zheng, X. B. Zhu, H. Wang, Y. A. Chen, C. Y. Lu, S. Y. Han, and J. W. Pan, 10-qubit entanglement and parallel logic operations with a superconducting circuit, *Phys. Rev. Lett.* **119**, 180511 (2017).
- [43] J. R. Johansson, P. D. Nation, and F. Nori, Qutip: An open-source Python framework for the dynamics of open quantum systems, *Comput. Phys. Commun.* **183**, 1760 (2012).
- [44] J. R. Johansson, P. D. Nation, and F. Nori, Qutip 2: A Python framework for the dynamics of open quantum systems, *Comput. Phys. Commun.* **184**, 1234 (2013).

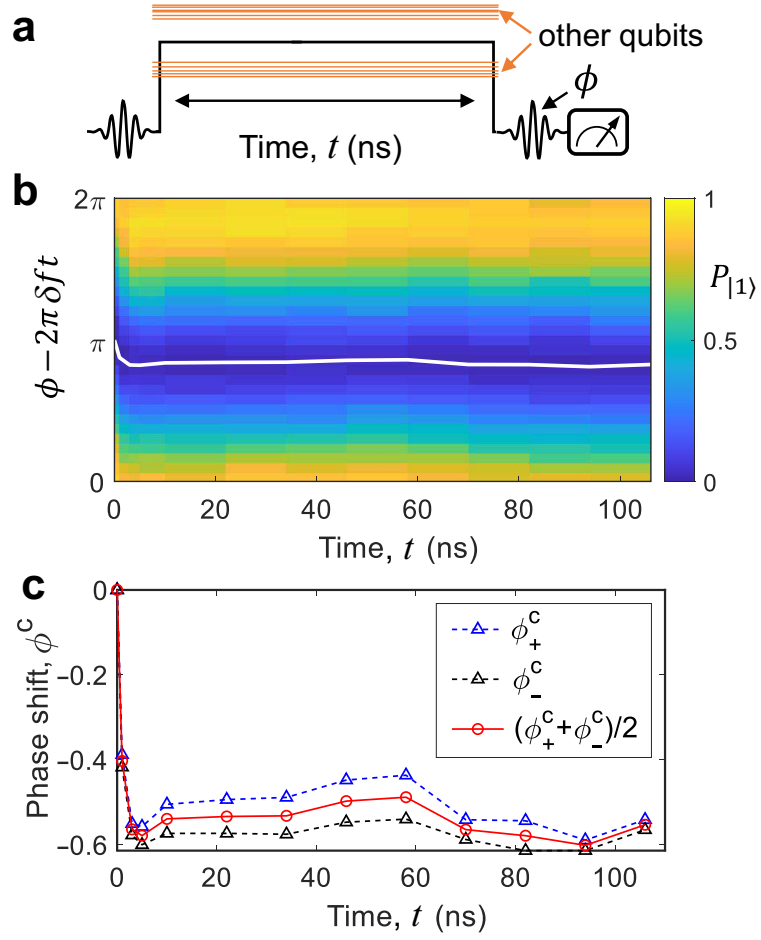


Extended Data Fig. 1. **Coupling matrix.** Plotted is the coupling strength  $\chi_{ij}/2\pi$  between  $q_i$  and  $q_j$  in the quantum processor, which is measured by the energy swapping process, where  $q_i$  and  $q_j$  are equally tuned at the working point  $\omega_I$  to interact for a specific time [42].

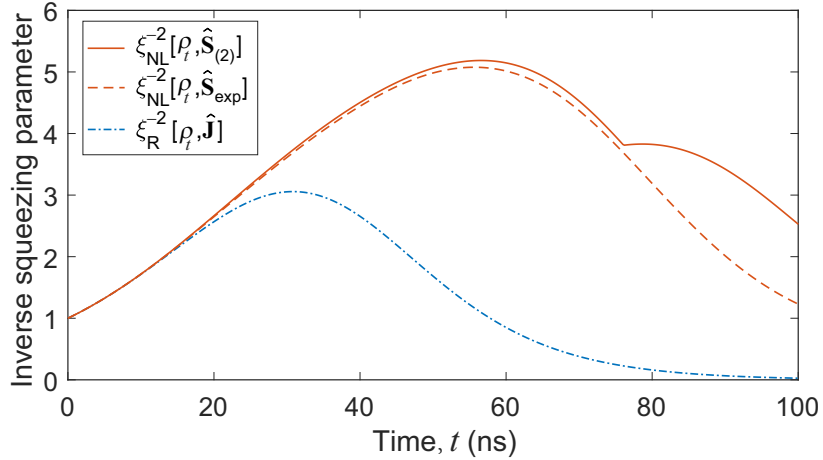


	$\omega_j/2\pi$ (GHz)	$T_{1,j}$ ( $\mu$ s)	$g_j/2\pi$ (MHz)	$\omega_j^r/2\pi$ (GHz)	$\omega_j^m/2\pi$ (GHz)	$F_{0,j}$	$F_{1,j}$
q <sub>1</sub>	4.350	$\approx 20$	27.6	6.768	4.460	0.977	0.921
q <sub>2</sub>	4.390	$\approx 26$	27.4	6.741	4.310	0.986	0.879
q <sub>3</sub>	4.275	$\approx 27$	29.1	6.707	4.355	0.975	0.912
q <sub>4</sub>	4.300	$\approx 26$	27.6	6.676	4.440	0.989	0.918
q <sub>5</sub>	4.245	$\approx 26$	26.5	6.649	4.260	0.975	0.909
q <sub>6</sub>	5.081	$\approx 27$	29.2	6.612	4.805	0.975	0.925
q <sub>8</sub>	4.215	$\approx 26$	30.1	6.558	4.285	0.987	0.906
q <sub>9</sub>	5.120	$\approx 23$	24.1	6.552	5.070	0.989	0.926
q <sub>10</sub>	5.160	$\approx 30$	27.7	6.514	5.290	0.995	0.903
q <sub>11</sub>	5.290	$\approx 24$	27.3	6.525	5.170	0.994	0.897
q <sub>12</sub>	5.215	$\approx 35$	26.9	6.550	5.210	0.981	0.920
q <sub>13</sub>	4.945	$\approx 26$	29.1	6.568	4.895	0.980	0.916
q <sub>14</sub>	5.250	$\approx 41$	27.4	6.598	5.250	0.983	0.896
q <sub>15</sub>	4.895	$\approx 31$	26.3	6.641	4.235	0.978	0.913
q <sub>16</sub>	4.325	$\approx 25$	26.5	6.660	4.850	0.987	0.934
q <sub>17</sub>	4.735	$\approx 36$	27.3	6.686	4.578	0.984	0.942
q <sub>18</sub>	4.815	$\approx 38$	29.0	6.713	4.770	0.982	0.912
q <sub>19</sub>	4.425	$\approx 35$	24.6	6.788	4.385	0.98	0.900
q <sub>20</sub>	4.855	$\approx 30$	27.5	6.759	5.115	0.985	0.918

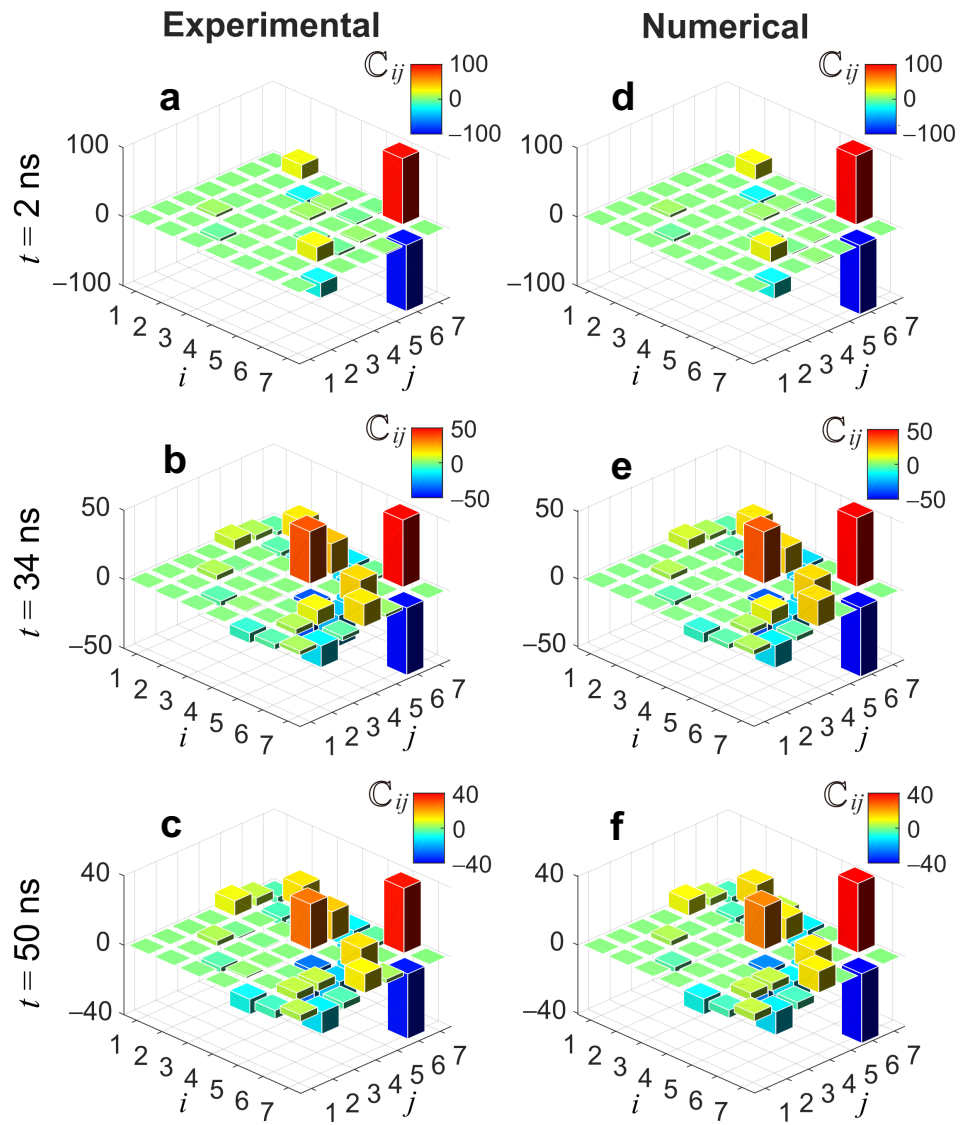
Extended Data Table I. **Qubit characteristics.**  $\omega_j/2\pi$  is the idle frequency of  $q_j$ , where single-qubit rotation pulses are applied.  $T_{1,j}$  is the energy relaxation time of  $q_j$ , which is the typical value across a wide frequency range.  $g_j/2\pi$  denotes the coupling strength between  $q_j$  and the resonator bus R.  $\omega_j^r/2\pi$  is the resonant frequency of  $q_j$ 's readout resonator.  $\omega_j^m/2\pi$  is the resonant frequency of  $q_j$  at the beginning of the measurement process, when its readout resonator is pumped with microwave pulse.  $F_{0,j}$  ( $F_{1,j}$ ) is the probability of detecting  $q_j$  in  $|0\rangle$  ( $|1\rangle$ ) state, when it is prepared in the  $|0\rangle$  ( $|1\rangle$ ) state.



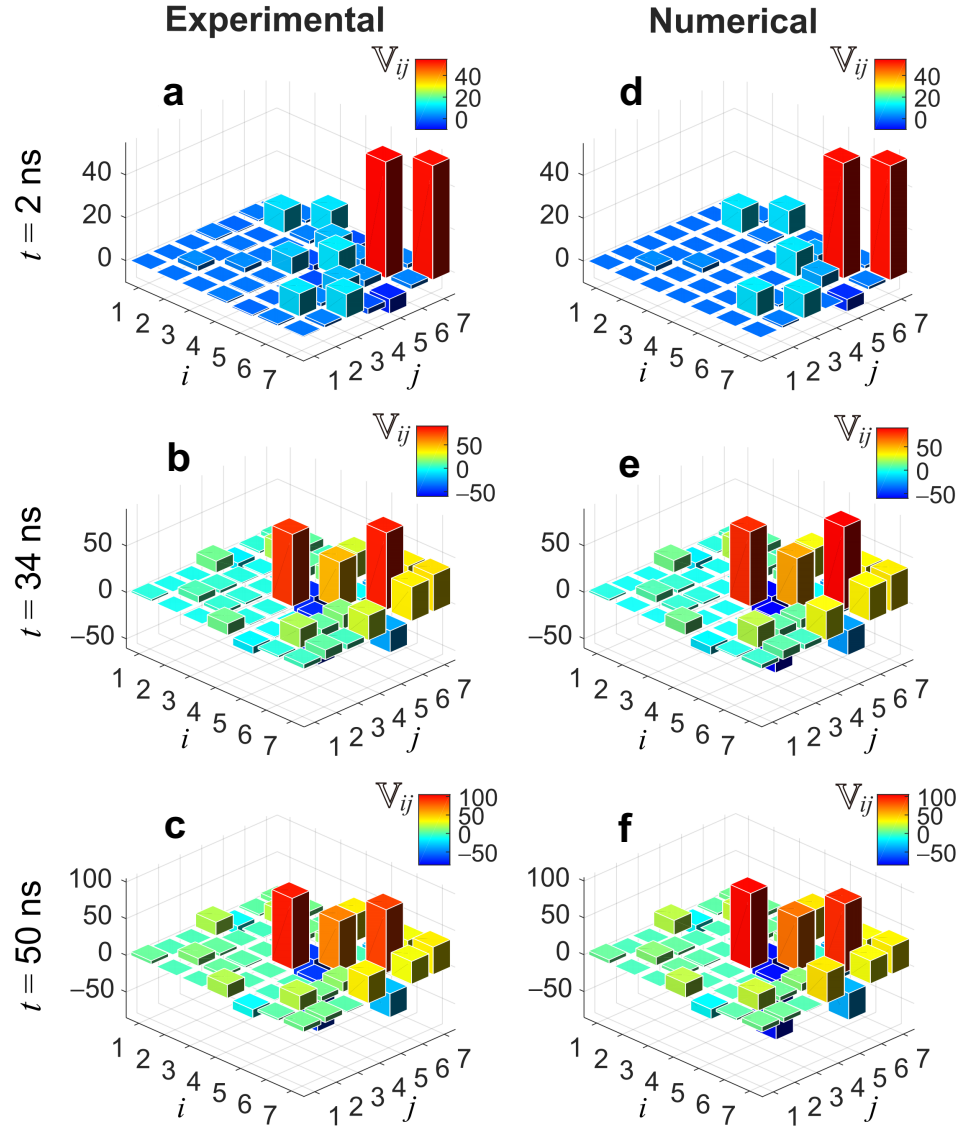
Extended Data Fig. 2. **Dynamical phase calibration.** **a**, Experimental results and sequence of phase calibration for  $q_1$ . **b**, The phase shift  $\phi^c$  obtained by fitting the results in (a) as a function of the interaction time  $t$ .



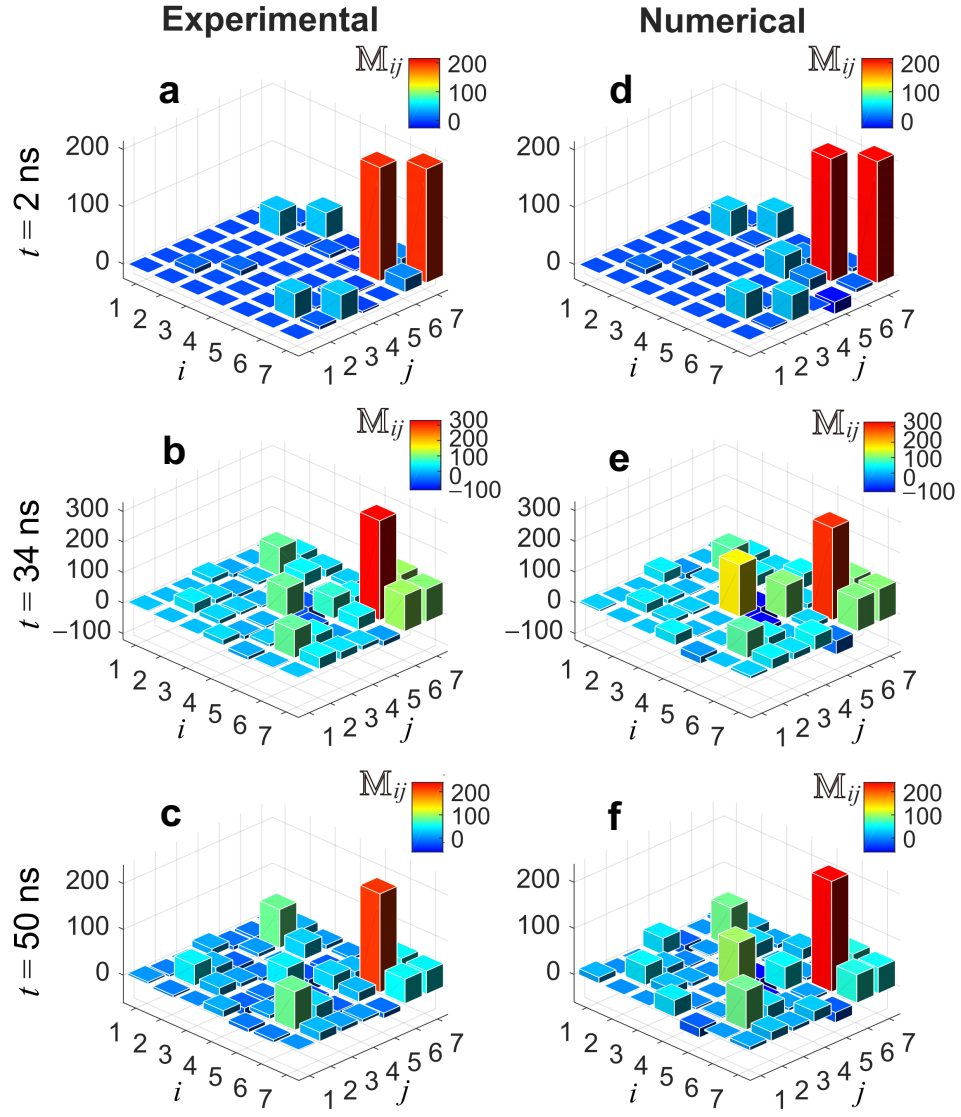
Extended Data Fig. 3. **Efficient detection of second-order nonlinear squeezing parameter with seven operators.** Numerical simulations of the evolutions of the inverse Ramsey squeezing parameter,  $\xi_{\text{R}}^{-2}[\rho_t, \hat{\mathbf{J}}]$ , with a family of 3 collective spin operators  $\hat{\mathbf{J}} = (\hat{J}_x, \hat{J}_y, \hat{J}_z)$ , the inverse second-order nonlinear squeezing parameter,  $\xi_{\text{NL}}^{-2}[\rho_t, \hat{S}_{(2)}]$ , with 9 operators in Eq. (10), and the inverse nonlinear squeezing parameter,  $\xi_{\text{NL}}^{-2}[\rho_t, \hat{S}_{\text{exp}}]$  with 7 operators in Eq. (9).



Extended Data Fig. 4. **Data of the  $C$  matrix.** **a-f**, Matrix  $C[\rho_t, \hat{S}_{\text{exp}}]$  experimentally measured at **(a)**  $t = 2$  ns, **(b)**  $t = 34$  ns, and **(c)**  $t = 50$  ns, compared with the numerical simulations **(d)**, **(e)**, and **(f)**.



Extended Data Fig. 5. **Data of the  $\mathbb{V}$  matrix.** **a-f**, Matrix  $\mathbb{V}[\rho_t, \hat{\mathbf{S}}_{\text{exp}}]$  experimentally measured at **(a)**  $t = 2$  ns, **(b)**  $t = 34$  ns, and **(c)**  $t = 50$  ns, compared with the numerical simulations **(d)**, **(e)**, and **(f)**.



Extended Data Fig. 6. **Data of the  $M$  matrix.** **a–f.** Matrix  $M[\rho_t, \hat{S}_{\text{exp}}]$  experimentally measured at **(a)**  $t = 2$  ns, **(b)**  $t = 34$  ns, and **(c)**  $t = 50$  ns, compared with the numerical simulations **(d)**, **(e)**, and **(f)**.

## Supplementary Information for: Metrological characterisation of non-Gaussian entangled states of superconducting qubits

Kai Xu,<sup>1,\*</sup> Yu-Ran Zhang,<sup>2,\*</sup> Zheng-Hang Sun,<sup>1,\*</sup> Hekang Li,<sup>1</sup> Pengtao Song,<sup>1</sup> Zhongcheng Xiang,<sup>1</sup> Kaixuan Huang,<sup>1</sup> Hao Li,<sup>1</sup> Yun-Hao Shi,<sup>1</sup> Chi-Tong Chen,<sup>1</sup> Xiaohui Song,<sup>1</sup> Dongning Zheng,<sup>1</sup> Franco Nori,<sup>2,3,†</sup> H. Wang,<sup>4,‡</sup> and Heng Fan<sup>1,5,§</sup>

<sup>1</sup>*Institute of Physics, Chinese Academy of Sciences, Beijing 100190, China*

<sup>2</sup>*Theoretical Quantum Physics Laboratory, RIKEN Cluster for Pioneering Research, Wako-shi, Saitama 351-0198, Japan*

<sup>3</sup>*Physics Department, University of Michigan, Ann Arbor, Michigan 48109-1040, USA*

<sup>4</sup>*Interdisciplinary Centre for Quantum Information, State Key Laboratory of Modern Optical Instrumentation, and Zhejiang Province Key Laboratory of Quantum Technology and Device, Department of Physics, Zhejiang University, Hangzhou 310027, China*

<sup>5</sup>*CAS Centre for Excellence in Topological Quantum Computation, UCAS, Beijing 100190, China*

### CONTENTS

I. Comparison of metrological gains over the quantum standard limit with other experiments	1
II. Measurement of linear and nonlinear spin squeezing parameters	3
A. Optimisation of metrological squeezing parameters	3
B. Linear Ramsey squeezing parameter	4
C. Second-order nonlinear squeezing parameter	5
D. Experimental details on measurement of squeezing parameters	9
III. Extraction of the Fisher information	10
A. Extraction of the Fisher information from the squared Hellinger distance	10
B. Experimental details for extracting the Fisher information	10
References	11

### I. COMPARISON OF METROLOGICAL GAINS OVER THE QUANTUM STANDARD LIMIT WITH OTHER EXPERIMENTS

Our experiments generate multiparticle entangled states of up to 19 superconducting qubits through the short-time nonlinear evolution of the system with the Hamiltonian in Eq. (1) of the main text. To characterise the useful entangled states for quantum metrology with superconducting qubits, we measure the linear and nonlinear spin squeezing parameters (discussed in Section II) and extract the Fisher information from the squared Hellinger distance (discussed in Section III), which all indicate the metrological gain over the quantum standard limit (SQL) of the phase sensitivity  $\Delta\theta_{\text{SQL}} \sim 1/\sqrt{N}$ , with  $N$  being the number of particles.

In our experiments, the Fisher information of non-Gaussian entangled states in the over-squeezed regime reveals the largest metrological gains. In Fig. S1, our experimental results,  $F/N = 7.10_{-0.28}^{+0.26}$  dB with  $N = 10$  qubits, and  $F/N = 9.89_{-0.29}^{+0.28}$  dB with  $N = 19$  qubits, are compared with other experimental results [1–35], obtained on different experimental platforms including cold/thermal atoms, trapped ions, Bose-Einstein condensates, photonic systems, Rydberg atoms, and superconducting qubits. Here, the experimental results in refs. [1–31] have been reviewed in Fig. 2 of ref. [36] (with the same list number). In addition, our comparison also includes several recent experimental results in refs. [32–35].

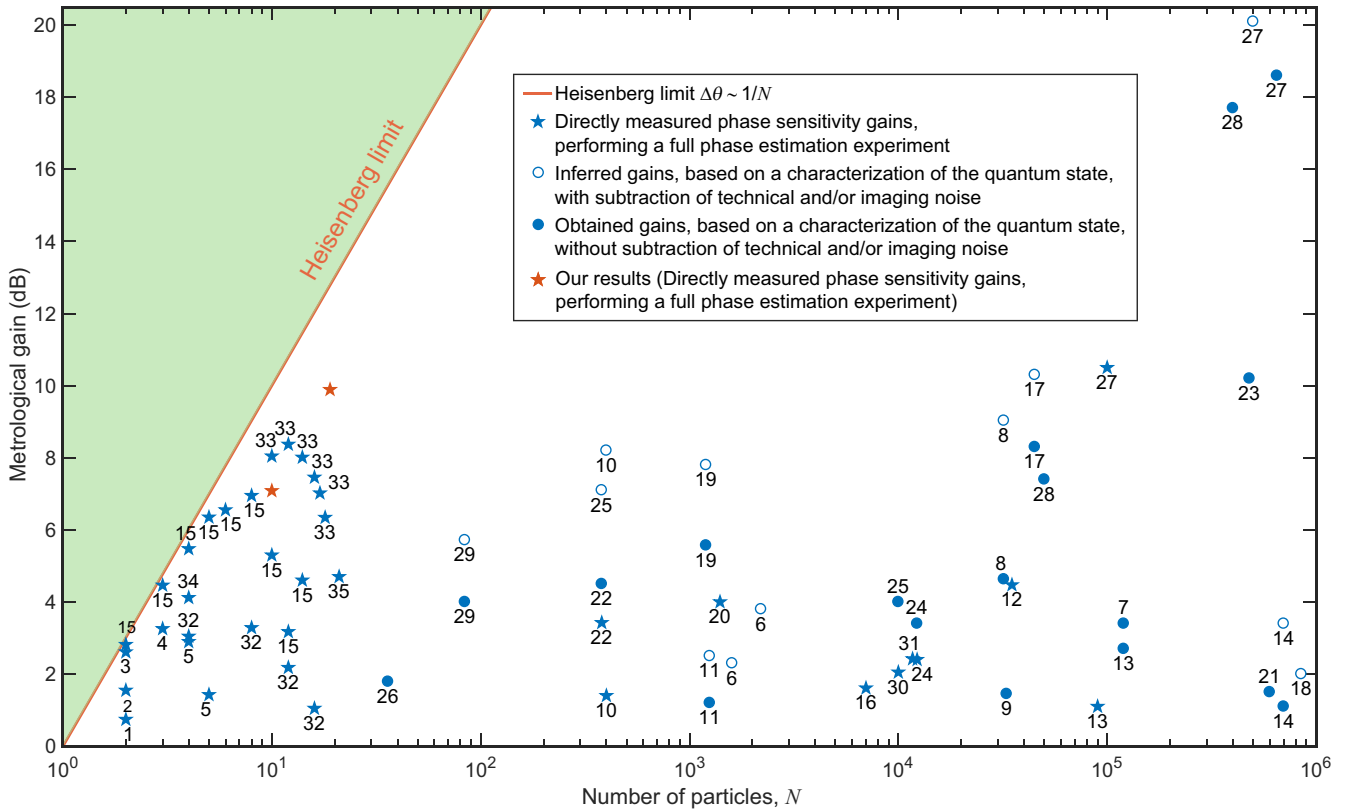
Our work shows that superconducting qubits, with high-fidelity controls and long decoherence times, are able to efficiently perform quantum metrology tasks, since our *metrological gain with 19 superconducting qubits is larger than the ones obtained on other platforms with up to 10,000 particles*. In addition, the ability to perform *single-shot readout measurement on each qubit* on the superconducting processor also makes the detection of *nonlinear* squeezing parameters and other quantum-information tasks possible. These advantages indicate the potential of an all-to-all connected superconducting circuit architecture for exploring quantum many-body physics, and also for practical applications in quantum metrology and quantum information processing.

\* These authors contributed equally to this work.

† [fnori@riken.jp](mailto:fnori@riken.jp)

‡ [hhwang@zju.edu.cn](mailto:hhwang@zju.edu.cn)

§ [hfan@iphy.ac.cn](mailto:hfan@iphy.ac.cn)



- [1] Sackett *et al.*, Nature **404**, 256 (2000).  
 [2] Meyer *et al.*, Phys. Rev. Lett. **86**, 5870 (2001).  
 [3] Leibfried *et al.*, Nature **422**, 412 (2003).  
 [4] Leibfried *et al.*, Science **304**, 1476 (2004).  
 [5] Leibfried *et al.*, Nature **438**, 639 (2005).  
 [6] Estève *et al.*, Nature **455**, 1216 (2008).  
 [7] Appel *et al.*, PNAS **106**, 10960 (2009).  
 [8] Leroux *et al.*, Phys. Rev. Lett. **104**, 073602 (2010).  
 [9] Schleier-Smith *et al.*, Phys. Rev. Lett. **104**, 073604 (2010).  
 [10] Gross *et al.*, Nature **464**, 1165 (2010).  
 [11] Riedel *et al.*, Nature **464**, 1170 (2010).  
 [12] Leroux *et al.*, Phys. Rev. Lett. **104**, 250801 (2010).  
 [13] Louchet-Chauvet *et al.*, New J. Phys. **12**, 065032 (2009).  
 [14] Chen *et al.*, Phys. Rev. Lett. **106**, 133601 (2011).  
 [15] Monz *et al.*, Phys. Rev. Lett. **106**, 130506 (2011).  
 [16] Lücke *et al.*, Science **334**, 773 (2011).  
 [17] Hamley *et al.*, Nat. Phys. **8**, 305 (2012).  
 [18] Sewell *et al.*, Phys. Rev. Lett. **109**, 253605 (2010).  
 [19] Berrada *et al.*, Nat. Commun. **4**, 2077 (2013).  
 [20] Ockeloen *et al.*, Phys. Rev. Lett. **111**, 143001 (2013).  
 [21] Sewell *et al.*, Phys. Rev. X **4**, 021045 (2014).  
 [22] Strobel *et al.*, Science **345**, 424 (2014).  
 [23] Bohnet *et al.*, Nat. Photon. **8**, 731 (2014).  
 [24] Muessel *et al.*, Phys. Rev. Lett. **113**, 103004 (2014).  
 [25] Muessel *et al.*, Phys. Rev. A **92**, 023603 (2015).  
 [26] Barontini *et al.*, Science **349**, 1317 (2015).  
 [27] Hosten *et al.*, Nature **529**, 505 (2016).  
 [28] Cox *et al.*, Phys. Rev. Lett. **116**, 093602 (2016).  
 [29] Bohnet *et al.*, Science **352**, 1297 (2016).  
 [30] Kruse *et al.*, Phys. Rev. Lett. **117**, 143004 (2016).  
 [31] Zou *et al.*, PNAS **115**, 6381 (2018).  
 [32] Omran *et al.*, Science **365**, 570 (2019).  
 [33] Song *et al.*, Science **365**, 574 (2019).  
 [34] Krischek *et al.*, Phys. Rev. Lett. **107**, 080504 (2011).  
 [35] Liu *et al.*, Nat. Photon. **15**, 137 (2021).

FIG. S1. **Metrological gains of the phase sensitivity over the standard quantum limit.** Comparing the metrological gains of phase sensitivity  $\Delta\theta$  over the standard quantum limit  $\Delta\theta_{\text{SQL}} \sim 1/\sqrt{N}$  with other experiments, which are shown on logarithmic scales,  $10 \log_{10}(\Delta\theta_{\text{SQL}}/\Delta\theta)^2$  dB. The solid red line shows the Heisenberg limit  $\Delta\theta_{\text{HL}} \sim 1/N$ . Each symbol is accompanied by a number, corresponding to the reference list below, where Refs. [1–31] are in the same order and displayed using the same data and symbols as in Ref. [36].

## II. MEASUREMENT OF LINEAR AND NONLINEAR SPIN SQUEEZING PARAMETERS

### A. Optimisation of metrological squeezing parameters

To estimate the phase  $\theta$ , imprinted on a state with a density matrix  $\rho_\theta$ , by measuring an observable  $\hat{X}$ , the phase sensitivity (for the unbiased estimation) can be given by [36]

$$\Delta^2\theta = \frac{1}{\nu} \frac{(\Delta_{\rho_\theta} \hat{X})^2}{(\partial_\theta \langle \hat{X} \rangle_{\rho_\theta})^2} \equiv \frac{\xi^2[\rho_\theta, \hat{X}]}{\nu}, \quad (\text{S1})$$

where  $\nu$  is the number of trials of the measurement. Here, the coefficient

$$\xi^2[\rho_\theta, \hat{X}] \equiv \frac{(\Delta_{\rho_\theta} \hat{X})^2}{(\partial_\theta \langle \hat{X} \rangle_{\rho_\theta})^2} \quad (\text{S2})$$

is defined as the metrological squeezing parameter of  $\rho$  with respect to the observable  $\hat{X}$  [37]. We consider the case that the phase is generated by a unitary process  $\rho_\theta = e^{-i\hat{G}\theta} \rho e^{i\hat{G}\theta}$  by a generator  $\hat{G}$ , and the squeezing parameter, in the limit  $\theta \rightarrow 0$ , can be obtained as

$$\xi^2[\rho, \hat{X}, \hat{G}] = \frac{(\Delta_\rho \hat{X})^2}{|\langle [\hat{X}, \hat{G}] \rangle_\rho|^2}, \quad (\text{S3})$$

where we have used the fact that  $(\Delta_{\rho_\theta} \hat{X})^2 \rightarrow (\Delta_\rho \hat{X})^2$ , and  $\partial_\theta \langle \hat{X} \rangle_{\rho_\theta} \rightarrow -i\langle [\hat{X}, \hat{G}] \rangle_\rho$ .

We then introduce a family of  $D$  accessible operators

$$\hat{\mathbf{S}} = (\hat{S}_1, \hat{S}_2, \hat{S}_3, \dots, \hat{S}_D), \quad (\text{S4})$$

with which the observable can be expressed as

$$\hat{X} = \hat{S}_{\hat{m}} = \hat{m} \cdot \hat{\mathbf{S}}, \quad (\text{S5})$$

with the unit vector  $\hat{m} \in \mathbb{R}^D$ . The generator is assumed to be a linear collective spin operator

$$\hat{G} = \hat{J}_{\hat{n}} = \hat{n} \cdot \hat{\mathbf{J}} \quad (\text{S6})$$

in the direction  $\hat{n} \in \mathbb{R}^3$  with the family of linear collective spin operators

$$\hat{\mathbf{J}} \equiv (\hat{J}_x, \hat{J}_y, \hat{J}_z). \quad (\text{S7})$$

Thus, the optimal metrological squeezing parameter for this family of operators can be written as

$$\xi_{\text{opt}}^2[\rho, \hat{\mathbf{S}}] = \min_{\hat{X} \in \text{span}(\hat{\mathbf{S}})} \min_{\hat{G} \in \text{span}(\hat{\mathbf{J}})} \xi^2[\rho, \hat{X}, \hat{G}] = \min_{\hat{m} \in \mathbb{R}^D} \min_{\hat{n} \in \mathbb{R}^3} \frac{N(\Delta_\rho \hat{S}_{\hat{m}})^2}{|\langle [\hat{S}_{\hat{m}}, \hat{J}_{\hat{n}}] \rangle_\rho|^2} = \frac{N}{\lambda_{\max}(\tilde{\mathbb{M}}[\rho, \hat{\mathbf{S}}])}, \quad (\text{S8})$$

where the last equality [Eq. (3) in the main text] is proved in ref. [37],  $N$  is the number of qubits, and  $\lambda_{\max}(\tilde{\mathbb{M}}[\rho, \hat{\mathbf{S}}])$  is the largest eigenvalue of a  $3 \times 3$  matrix  $\tilde{\mathbb{M}}[\rho, \hat{\mathbf{S}}]$ . The matrix  $\tilde{\mathbb{M}}[\rho, \hat{\mathbf{S}}]$  contains the first three rows and columns of a  $D \times D$  matrix as

$$\mathbb{M}[\rho, \hat{\mathbf{S}}] = \mathbb{C}^T[\rho, \hat{\mathbf{S}}] \mathbb{V}^{-1}[\rho, \hat{\mathbf{S}}] \mathbb{C}[\rho, \hat{\mathbf{S}}], \quad (\text{S9})$$

where  $\mathbb{V}[\rho, \hat{\mathbf{S}}]$  is the covariance matrix (symmetric,  $\mathbb{V}^T = \mathbb{V}$ ) with elements:

$$\mathbb{V}_{ij}[\rho, \hat{\mathbf{S}}] = \text{Cov}_\rho(\hat{S}_i, \hat{S}_j) = \frac{\langle \{\hat{S}_i, \hat{S}_j\} \rangle_\rho}{2} - \langle \hat{S}_i \rangle_\rho \langle \hat{S}_j \rangle_\rho, \quad (\text{S10})$$

and  $\mathbb{C}[\rho, \hat{\mathbf{H}}]$  is the real-valued skew-symmetric commutator matrix (asymmetric,  $\mathbb{C}^T = -\mathbb{C}$ ) with elements:

$$\mathbb{C}_{ij}[\rho, \hat{\mathbf{S}}] = -i\langle [\hat{S}_i, \hat{S}_j] \rangle_\rho. \quad (\text{S11})$$



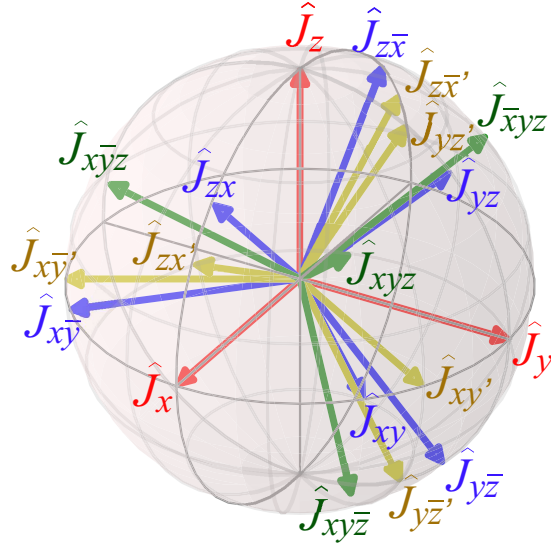


FIG. S2. **Directions of collective spin operators for single-shot readout measurements.** The collective spin operators to obtain the second-order nonlinear squeezing parameter via performing the single-shot readout measurement on each superconducting qubit:  $\{\hat{J}_x, \hat{J}_y, \hat{J}_z, \hat{J}_{xy}, \hat{J}_{yz}, \hat{J}_{zx}, \hat{J}_{x\bar{y}}, \hat{J}_{y\bar{z}}, \hat{J}_{z\bar{x}}, \hat{J}_{xy'}, \hat{J}_{yz'}, \hat{J}_{zx'}, \hat{J}_{x\bar{y}'}, \hat{J}_{y\bar{z}'}, \hat{J}_{z\bar{x}'}, \hat{J}_{xy\bar{z}}, \hat{J}_{x\bar{y}z}, \hat{J}_{y\bar{z}x}, \hat{J}_{x\bar{y}\bar{z}}\}$ , as shown in Eqs. (S19–S23). The unit vectors for the directions of these collective spin operators are plotted in a unit sphere.

### B. Linear Ramsey squeezing parameter

To optimise the linear Ramsey squeezing parameter using Eq. (S8), we consider the accessible operators as spanned by a family of collective spin operators

$$\hat{\mathbf{S}}_{(1)} \equiv \hat{\mathbf{J}} = (\hat{J}_x, \hat{J}_y, \hat{J}_z)_{D=3}. \quad (\text{S12})$$

Then, the optimal spin squeezed parameter can be calculated with matrices

$$\mathbb{V}_{(1)} = \begin{pmatrix} (\Delta_\rho \hat{J}_x)^2 & \text{cov}_\rho(\hat{J}_x, \hat{J}_y) & \text{cov}_\rho(\hat{J}_x, \hat{J}_z) \\ \vdots & (\Delta_\rho \hat{J}_y)^2 & \text{cov}_\rho(\hat{J}_y, \hat{J}_z) \\ \dots & \dots & (\Delta_\rho \hat{J}_z)^2 \end{pmatrix}, \quad (\text{S13})$$

$$\mathbb{C}_{(1)} = \begin{pmatrix} 0 & \langle \hat{J}_z \rangle_\rho & -\langle \hat{J}_y \rangle_\rho \\ -\langle \hat{J}_z \rangle_\rho & 0 & \langle \hat{J}_x \rangle_\rho \\ \langle \hat{J}_y \rangle_\rho & -\langle \hat{J}_x \rangle_\rho & 0 \end{pmatrix}, \quad (\text{S14})$$

where, e.g., the covariance  $\text{cov}_\rho(\hat{J}_x, \hat{J}_y)$  can be measured by the single-shot readout measurement of the observable operator  $\hat{J}_{xy} \equiv (\hat{J}_x + \hat{J}_y)/\sqrt{2}$  with

$$\text{cov}_\rho(\hat{J}_x, \hat{J}_y) = \langle \hat{J}_{xy}^2 \rangle_\rho - \frac{\langle \hat{J}_x^2 \rangle_\rho + \langle \hat{J}_y^2 \rangle_\rho}{2} - \langle \hat{J}_x \rangle_\rho \langle \hat{J}_y \rangle_\rho, \quad (\text{S15})$$

$$\text{cov}_\rho(\hat{J}_x, \hat{J}_z) = \langle \hat{J}_{zx}^2 \rangle_\rho - \frac{\langle \hat{J}_x^2 \rangle_\rho + \langle \hat{J}_z^2 \rangle_\rho}{2} - \langle \hat{J}_x \rangle_\rho \langle \hat{J}_z \rangle_\rho, \quad (\text{S16})$$

$$\text{cov}_\rho(\hat{J}_y, \hat{J}_z) = \langle \hat{J}_{yz}^2 \rangle_\rho - \frac{\langle \hat{J}_y^2 \rangle_\rho + \langle \hat{J}_z^2 \rangle_\rho}{2} - \langle \hat{J}_y \rangle_\rho \langle \hat{J}_z \rangle_\rho. \quad (\text{S17})$$

### C. Second-order nonlinear squeezing parameter

For the second-order nonlinear squeezing parameter, we introduce a family of  $D = 9$  linear and quadratic collective spin operators,

$$\hat{\mathbf{S}}_{(2)} = (\hat{J}_x, \hat{J}_y, \hat{J}_z, \hat{J}_x^2, \hat{J}_y^2, \hat{J}_z^2, \hat{J}_{xy}^2, \hat{J}_{yz}^2, \hat{J}_{zx}^2)_{D=9}, \quad (\text{S18})$$

with the single-shot readout measurements of the operators, as shown in Fig. S2 with direction vectors on a unit sphere.

$$\hat{J}_x, \hat{J}_y, \hat{J}_z \quad (\text{S19})$$

$$\hat{J}_{xy} = \frac{\hat{J}_x + \hat{J}_y}{\sqrt{2}}, \quad \hat{J}_{yz} = \frac{\hat{J}_y + \hat{J}_z}{\sqrt{2}}, \quad \hat{J}_{zx} = \frac{\hat{J}_x + \hat{J}_z}{\sqrt{2}}, \quad \hat{J}_{x\bar{y}} = \frac{\hat{J}_x - \hat{J}_y}{\sqrt{2}}, \quad \hat{J}_{y\bar{z}} = \frac{\hat{J}_y - \hat{J}_z}{\sqrt{2}}, \quad \hat{J}_{z\bar{x}} = \frac{\hat{J}_z - \hat{J}_x}{\sqrt{2}}, \quad (\text{S20})$$

$$\hat{J}_{xy'} = \frac{\hat{J}_x + \sqrt{3}\hat{J}_y}{2}, \quad \hat{J}_{yz'} = \frac{\hat{J}_y + \sqrt{3}\hat{J}_z}{2}, \quad \hat{J}_{zx'} = \frac{\hat{J}_z + \sqrt{3}\hat{J}_x}{2}, \quad (\text{S21})$$

$$\hat{J}_{x\bar{y}'} = \frac{\hat{J}_x - \sqrt{3}\hat{J}_y}{2}, \quad \hat{J}_{y\bar{z}'} = \frac{\hat{J}_y - \sqrt{3}\hat{J}_z}{2}, \quad \hat{J}_{z\bar{x}'} = \frac{\hat{J}_z - \sqrt{3}\hat{J}_x}{2}, \quad (\text{S22})$$

$$\hat{J}_{xyz} = \frac{\hat{J}_x + \hat{J}_y + \hat{J}_z}{\sqrt{3}}, \quad \hat{J}_{x\bar{y}z} = \frac{-\hat{J}_x + \hat{J}_y + \hat{J}_z}{\sqrt{3}}, \quad \hat{J}_{x\bar{y}\bar{z}} = \frac{\hat{J}_x - \hat{J}_y + \hat{J}_z}{\sqrt{3}}, \quad \hat{J}_{xy\bar{z}} = \frac{\hat{J}_x + \hat{J}_y - \hat{J}_z}{\sqrt{3}}. \quad (\text{S23})$$

The covariance matrix  $\mathbb{V}_{(2)}$  for the second-order spin squeezing parameter is written as

$$\mathbb{V}_{(2)} = \left( \begin{array}{c|ccc|ccc} & \text{cov}_\rho(J_x, J_x^2) & \text{cov}_\rho(\hat{J}_x, \hat{J}_y^2) & \text{cov}_\rho(\hat{J}_x, \hat{J}_z^2) & \text{cov}_\rho(\hat{J}_x, \hat{J}_{xy}^2) & \text{cov}_\rho(\hat{J}_x, \hat{J}_{yz}^2) & \text{cov}_\rho(\hat{J}_x, \hat{J}_{zx}^2) \\ \mathbb{V}_{(1)} & \text{cov}_\rho(\hat{J}_y, \hat{J}_x^2) & \text{cov}_\rho(\hat{J}_y, \hat{J}_y^2) & \text{cov}_\rho(\hat{J}_y, \hat{J}_z^2) & \text{cov}_\rho(\hat{J}_y, \hat{J}_{xy}^2) & \text{cov}_\rho(\hat{J}_y, \hat{J}_{yz}^2) & \text{cov}_\rho(\hat{J}_y, \hat{J}_{zx}^2) \\ & \text{cov}_\rho(\hat{J}_z, \hat{J}_x^2) & \text{cov}_\rho(\hat{J}_z, \hat{J}_y^2) & \text{cov}_\rho(\hat{J}_z, \hat{J}_z^2) & \text{cov}_\rho(\hat{J}_z, \hat{J}_{xy}^2) & \text{cov}_\rho(\hat{J}_z, \hat{J}_{yz}^2) & \text{cov}_\rho(\hat{J}_z, \hat{J}_{zx}^2) \\ \hline & (\Delta_\rho \hat{J}_x^2)^2 & \text{cov}_\rho(\hat{J}_x^2, \hat{J}_y^2) & \text{cov}_\rho(\hat{J}_x^2, \hat{J}_z^2) & \text{cov}_\rho(\hat{J}_x^2, \hat{J}_{xy}^2) & \text{cov}_\rho(\hat{J}_x^2, \hat{J}_{yz}^2) & \text{cov}_\rho(\hat{J}_x^2, \hat{J}_{zx}^2) \\ \vdots & \vdots & (\Delta_\rho \hat{J}_y^2)^2 & \text{cov}_\rho(\hat{J}_y^2, \hat{J}_z^2) & \text{cov}_\rho(\hat{J}_y^2, \hat{J}_{xy}^2) & \text{cov}_\rho(\hat{J}_y^2, \hat{J}_{yz}^2) & \text{cov}_\rho(\hat{J}_y^2, \hat{J}_{zx}^2) \\ & \cdots & \cdots & (\Delta_\rho \hat{J}_z^2)^2 & \text{cov}_\rho(\hat{J}_z^2, \hat{J}_{xy}^2) & \text{cov}_\rho(\hat{J}_z^2, \hat{J}_{yz}^2) & \text{cov}_\rho(\hat{J}_z^2, \hat{J}_{zx}^2) \\ \hline \vdots & \cdots & \cdots & \cdots & (\Delta_\rho \hat{J}_{xy}^2)^2 & \text{cov}_\rho(\hat{J}_{xy}^2, \hat{J}_{yz}^2) & \text{cov}_\rho(\hat{J}_{xy}^2, \hat{J}_{zx}^2) \\ & \cdots & \cdots & \cdots & \vdots & (\Delta_\rho \hat{J}_{yz}^2)^2 & \text{cov}_\rho(\hat{J}_{yz}^2, \hat{J}_{zx}^2) \\ & & & & \cdots & \cdots & (\Delta_\rho \hat{J}_{zx}^2)^2 \end{array} \right), \quad (\text{S24})$$

with some of the elements being written in terms of the averages of measurable observables, as listed below: [We have shown the elements for the first three rows and columns in Eqs. (S13).]

$$\text{cov}_\rho(\hat{J}_x^2, \hat{J}_y^2) = [2(\langle \hat{J}_{xy}^4 \rangle_\rho + \langle \hat{J}_{x\bar{y}}^4 \rangle_\rho) - \langle \hat{J}_x^4 \rangle_\rho - \langle \hat{J}_y^4 \rangle_\rho - 3\langle \hat{J}_z^2 \rangle_\rho + 2\langle \hat{J}_y^2 \rangle_\rho + 2\langle \hat{J}_x^2 \rangle_\rho]/6 - \langle \hat{J}_x^2 \rangle_\rho \langle \hat{J}_y^2 \rangle_\rho, \quad (\text{S25})$$

$$\text{cov}_\rho(\hat{J}_x^2, \hat{J}_z^2) = [2(\langle \hat{J}_{zx}^4 \rangle_\rho + \langle \hat{J}_{z\bar{x}}^4 \rangle_\rho) - \langle \hat{J}_x^4 \rangle_\rho - \langle \hat{J}_z^4 \rangle_\rho - 3\langle \hat{J}_y^2 \rangle_\rho + 2\langle \hat{J}_x^2 \rangle_\rho + 2\langle \hat{J}_z^2 \rangle_\rho]/6 - \langle \hat{J}_x^2 \rangle_\rho \langle \hat{J}_z^2 \rangle_\rho, \quad (\text{S26})$$

$$\text{cov}_\rho(\hat{J}_y^2, \hat{J}_z^2) = [2(\langle \hat{J}_{yz}^4 \rangle_\rho + \langle \hat{J}_{y\bar{z}}^4 \rangle_\rho) - \langle \hat{J}_y^4 \rangle_\rho - \langle \hat{J}_z^4 \rangle_\rho - 3\langle \hat{J}_x^2 \rangle_\rho + 2\langle \hat{J}_y^2 \rangle_\rho + 2\langle \hat{J}_z^2 \rangle_\rho]/6 - \langle \hat{J}_y^2 \rangle_\rho \langle \hat{J}_z^2 \rangle_\rho, \quad (\text{S27})$$

and

$$\text{cov}_\rho(\hat{J}_x, \hat{J}_y^2) = [\sqrt{2}(\langle \hat{J}_{xy}^3 \rangle_\rho + \langle \hat{J}_{x\bar{y}}^3 \rangle_\rho) - \langle \hat{J}_x^3 \rangle_\rho + \langle \hat{J}_y \rangle_\rho]/3 - \langle \hat{J}_x \rangle_\rho \langle \hat{J}_y^2 \rangle_\rho, \quad (\text{S28})$$

$$\text{cov}_\rho(\hat{J}_y, \hat{J}_z^2) = [\sqrt{2}(\langle \hat{J}_{yz}^3 \rangle_\rho + \langle \hat{J}_{y\bar{z}}^3 \rangle_\rho) - \langle \hat{J}_y^3 \rangle_\rho + \langle \hat{J}_z \rangle_\rho]/3 - \langle \hat{J}_y \rangle_\rho \langle \hat{J}_z^2 \rangle_\rho, \quad (\text{S29})$$

$$\text{cov}_\rho(\hat{J}_z, \hat{J}_x^2) = [\sqrt{2}(\langle \hat{J}_{zx}^3 \rangle_\rho + \langle \hat{J}_{z\bar{x}}^3 \rangle_\rho) - \langle \hat{J}_z^3 \rangle_\rho + \langle \hat{J}_x \rangle_\rho]/3 - \langle \hat{J}_z \rangle_\rho \langle \hat{J}_x^2 \rangle_\rho, \quad (\text{S30})$$

$$\text{cov}_\rho(\hat{J}_x, \hat{J}_z^2) = [\sqrt{2}(\langle \hat{J}_{zx}^3 \rangle_\rho - \langle \hat{J}_{z\bar{x}}^3 \rangle_\rho) - \langle \hat{J}_x^3 \rangle_\rho + \langle \hat{J}_z \rangle_\rho]/3 - \langle \hat{J}_x \rangle_\rho \langle \hat{J}_z^2 \rangle_\rho, \quad (\text{S31})$$

$$\text{cov}_\rho(\hat{J}_y, \hat{J}_x^2) = [\sqrt{2}(\langle \hat{J}_{xy}^3 \rangle_\rho - \langle \hat{J}_{x\bar{y}}^3 \rangle_\rho) - \langle \hat{J}_y^3 \rangle_\rho + \langle \hat{J}_x \rangle_\rho]/3 - \langle \hat{J}_y \rangle_\rho \langle \hat{J}_x^2 \rangle_\rho, \quad (\text{S32})$$

$$\text{cov}_\rho(\hat{J}_z, \hat{J}_y^2) = [\sqrt{2}(\langle \hat{J}_{yz}^3 \rangle_\rho - \langle \hat{J}_{y\bar{z}}^3 \rangle_\rho) - \langle \hat{J}_z^3 \rangle_\rho + \langle \hat{J}_y \rangle_\rho]/3 - \langle \hat{J}_z \rangle_\rho \langle \hat{J}_y^2 \rangle_\rho, \quad (\text{S33})$$





The skew-symmetric commutator matrix is written as

$$\mathbb{C} = -i \left\langle \begin{array}{c|cc} 0 & [\hat{J}_x, \hat{J}_y] & [\hat{J}_x, \hat{J}_z] \\ & 0 & [\hat{J}_y, \hat{J}_z] \\ \hline & [\hat{J}_y, \hat{J}_x] & 0 \\ & [\hat{J}_z, \hat{J}_x] & [\hat{J}_z, \hat{J}_y] \\ \hline & 0 & [\hat{J}_x^2, \hat{J}_y^2] \\ & & 0 \\ \hline & & 0 \\ & & 0 \\ \hline & & 0 \\ & [\hat{J}_{xy}^2, \hat{J}_{yz}^2] & [\hat{J}_{xy}^2, \hat{J}_{zx}^2] \\ & & 0 \\ & & [\hat{J}_{yz}^2, \hat{J}_{zx}^2] \\ & & 0 \end{array} \right\rangle_{\rho}, \quad (\text{S55})$$

with elements

$$-i \langle [\hat{J}_x, \hat{J}_y] \rangle_{\rho} = \langle \hat{J}_z \rangle_{\rho}, \quad -i \langle [\hat{J}_x, \hat{J}_z] \rangle_{\rho} = -\langle \hat{J}_y \rangle_{\rho}, \quad -i \langle [\hat{J}_y, \hat{J}_z] \rangle_{\rho} = \langle \hat{J}_x \rangle_{\rho}, \quad (\text{S56})$$

$$-i \langle [\hat{J}_x, \hat{J}_y^2] \rangle_{\rho} = 2 \langle \hat{J}_{yz}^2 \rangle_{\rho} - \langle \hat{J}_y^2 \rangle_{\rho} - \langle \hat{J}_z^2 \rangle_{\rho}, \quad -i \langle [\hat{J}_x, \hat{J}_z^2] \rangle_{\rho} = 2 \langle \hat{J}_{y\bar{z}}^2 \rangle_{\rho} - \langle \hat{J}_y^2 \rangle_{\rho} - \langle \hat{J}_z^2 \rangle_{\rho}, \quad (\text{S57})$$

$$-i \langle [\hat{J}_y, \hat{J}_z^2] \rangle_{\rho} = 2 \langle \hat{J}_{zx}^2 \rangle_{\rho} - \langle \hat{J}_z^2 \rangle_{\rho} - \langle \hat{J}_x^2 \rangle_{\rho}, \quad -i \langle [\hat{J}_y, \hat{J}_x^2] \rangle_{\rho} = 2 \langle \hat{J}_{z\bar{x}}^2 \rangle_{\rho} - \langle \hat{J}_z^2 \rangle_{\rho} - \langle \hat{J}_x^2 \rangle_{\rho}, \quad (\text{S58})$$

$$-i \langle [\hat{J}_z, \hat{J}_x^2] \rangle_{\rho} = 2 \langle \hat{J}_{xy}^2 \rangle_{\rho} - \langle \hat{J}_x^2 \rangle_{\rho} - \langle \hat{J}_y^2 \rangle_{\rho}, \quad -i \langle [\hat{J}_z, \hat{J}_y^2] \rangle_{\rho} = 2 \langle \hat{J}_{x\bar{y}}^2 \rangle_{\rho} - \langle \hat{J}_x^2 \rangle_{\rho} - \langle \hat{J}_y^2 \rangle_{\rho}, \quad (\text{S59})$$

and

$$-i \langle [\hat{J}_x^2, \hat{J}_y^2] \rangle_{\rho} = 2\sqrt{3} \langle \hat{J}_{xyz}^3 \rangle_{\rho} - \frac{4\sqrt{2}(\langle \hat{J}_{xy}^3 \rangle_{\rho} + \langle \hat{J}_{yz}^3 \rangle_{\rho} + \langle \hat{J}_{zx}^3 \rangle_{\rho})}{3} + \frac{2(\langle \hat{J}_x^3 \rangle_{\rho} + \langle \hat{J}_y^3 \rangle_{\rho} + \langle \hat{J}_z^3 \rangle_{\rho})}{3}, \quad (\text{S60})$$

$$-i \langle [\hat{J}_x^2, \hat{J}_z^2] \rangle_{\rho} = i \langle [\hat{J}_x^2, \hat{J}_y^2] \rangle_{\rho}, \quad (\text{S61})$$

$$-i \langle [\hat{J}_y^2, \hat{J}_z^2] \rangle_{\rho} = -i \langle [\hat{J}_x^2, \hat{J}_y^2] \rangle_{\rho}, \quad (\text{S62})$$

to further obtain that

$$-i \langle [\hat{J}_x, \hat{J}_{xy}^2] \rangle_{\rho} = \frac{i}{2} \langle [\hat{J}_y, \hat{J}_x^2] \rangle_{\rho} - \frac{i}{2} \langle [\hat{J}_x, \hat{J}_y^2] \rangle_{\rho}, \quad -i \langle [\hat{J}_x, \hat{J}_{zx}^2] \rangle_{\rho} = \frac{i}{2} \langle [\hat{J}_z, \hat{J}_x^2] \rangle_{\rho} - \frac{i}{2} \langle [\hat{J}_x, \hat{J}_z^2] \rangle_{\rho}, \quad (\text{S63})$$

$$-i \langle [\hat{J}_y, \hat{J}_{xy}^2] \rangle_{\rho} = \frac{i}{2} \langle [\hat{J}_x, \hat{J}_y^2] \rangle_{\rho} - \frac{i}{2} \langle [\hat{J}_y, \hat{J}_x^2] \rangle_{\rho}, \quad -i \langle [\hat{J}_y, \hat{J}_{yz}^2] \rangle_{\rho} = \frac{i}{2} \langle [\hat{J}_z, \hat{J}_y^2] \rangle_{\rho} - \frac{i}{2} \langle [\hat{J}_y, \hat{J}_z^2] \rangle_{\rho}, \quad (\text{S64})$$

$$-i \langle [\hat{J}_z, \hat{J}_{yz}^2] \rangle_{\rho} = \frac{i}{2} \langle [\hat{J}_y, \hat{J}_z^2] \rangle_{\rho} - \frac{i}{2} \langle [\hat{J}_z, \hat{J}_y^2] \rangle_{\rho}, \quad -i \langle [\hat{J}_z, \hat{J}_{zx}^2] \rangle_{\rho} = \frac{i}{2} \langle [\hat{J}_x, \hat{J}_z^2] \rangle_{\rho} - \frac{i}{2} \langle [\hat{J}_z, \hat{J}_x^2] \rangle_{\rho}, \quad (\text{S65})$$

and

$$-i \langle [\hat{J}_x, \hat{J}_{yz}^2] \rangle_{\rho} = -\frac{i}{2} \langle [\hat{J}_x, \hat{J}_y^2] \rangle_{\rho} - \frac{i}{2} \langle [\hat{J}_x, \hat{J}_z^2] \rangle_{\rho} + \langle \hat{J}_z^2 \rangle_{\rho} - \langle \hat{J}_y^2 \rangle_{\rho}, \quad (\text{S66})$$

$$-i \langle [\hat{J}_y, \hat{J}_{zx}^2] \rangle_{\rho} = -\frac{i}{2} \langle [\hat{J}_y, \hat{J}_z^2] \rangle_{\rho} - \frac{i}{2} \langle [\hat{J}_y, \hat{J}_x^2] \rangle_{\rho} + \langle \hat{J}_x^2 \rangle_{\rho} - \langle \hat{J}_z^2 \rangle_{\rho}, \quad (\text{S67})$$

$$-i \langle [\hat{J}_z, \hat{J}_{xy}^2] \rangle_{\rho} = -\frac{i}{2} \langle [\hat{J}_z, \hat{J}_x^2] \rangle_{\rho} - \frac{i}{2} \langle [\hat{J}_z, \hat{J}_y^2] \rangle_{\rho} + \langle \hat{J}_y^2 \rangle_{\rho} - \langle \hat{J}_x^2 \rangle_{\rho}, \quad (\text{S68})$$

and

$$-i \langle [\hat{J}_x^2, \hat{J}_{xy}^2] \rangle_{\rho} = \frac{2\sqrt{2}(\langle \hat{J}_{zx}^3 \rangle_{\rho} + \langle \hat{J}_{z\bar{x}}^3 \rangle_{\rho})}{3} - \frac{2\langle \hat{J}_z^3 \rangle_{\rho}}{3} - \frac{\langle \hat{J}_z \rangle_{\rho}}{6} - \frac{i}{2} \langle [\hat{J}_x^2, \hat{J}_y^2] \rangle_{\rho}, \quad (\text{S69})$$

$$-i \langle [\hat{J}_y^2, \hat{J}_{yz}^2] \rangle_{\rho} = \frac{2\sqrt{2}(\langle \hat{J}_{xy}^3 \rangle_{\rho} + \langle \hat{J}_{x\bar{y}}^3 \rangle_{\rho})}{3} - \frac{2\langle \hat{J}_x^3 \rangle_{\rho}}{3} - \frac{\langle \hat{J}_x \rangle_{\rho}}{6} - \frac{i}{2} \langle [\hat{J}_y^2, \hat{J}_z^2] \rangle_{\rho}, \quad (\text{S70})$$

$$-i \langle [\hat{J}_z^2, \hat{J}_{zx}^2] \rangle_{\rho} = \frac{2\sqrt{2}(\langle \hat{J}_{yz}^3 \rangle_{\rho} + \langle \hat{J}_{y\bar{z}}^3 \rangle_{\rho})}{3} - \frac{2\langle \hat{J}_y^3 \rangle_{\rho}}{3} - \frac{\langle \hat{J}_y \rangle_{\rho}}{6} - \frac{i}{2} \langle [\hat{J}_z^2, \hat{J}_x^2] \rangle_{\rho}, \quad (\text{S71})$$

$$-i \langle [\hat{J}_x^2, \hat{J}_{zx}^2] \rangle_{\rho} = -\frac{2\sqrt{2}(\langle \hat{J}_{xy}^3 \rangle_{\rho} - \langle \hat{J}_{x\bar{y}}^3 \rangle_{\rho})}{3} + \frac{2\langle \hat{J}_y^3 \rangle_{\rho}}{3} + \frac{\langle \hat{J}_y \rangle_{\rho}}{6} - \frac{i}{2} \langle [\hat{J}_x^2, \hat{J}_z^2] \rangle_{\rho}, \quad (\text{S72})$$

$$-i \langle [\hat{J}_y^2, \hat{J}_{xy}^2] \rangle_{\rho} = -\frac{2\sqrt{2}(\langle \hat{J}_{yz}^3 \rangle_{\rho} - \langle \hat{J}_{y\bar{z}}^3 \rangle_{\rho})}{3} + \frac{2\langle \hat{J}_x^3 \rangle_{\rho}}{3} + \frac{\langle \hat{J}_z \rangle_{\rho}}{6} - \frac{i}{2} \langle [\hat{J}_y^2, \hat{J}_x^2] \rangle_{\rho}, \quad (\text{S73})$$

$$-i \langle [\hat{J}_z^2, \hat{J}_{yz}^2] \rangle_{\rho} = -\frac{2\sqrt{2}(\langle \hat{J}_{zx}^3 \rangle_{\rho} - \langle \hat{J}_{z\bar{x}}^3 \rangle_{\rho})}{3} + \frac{2\langle \hat{J}_x^3 \rangle_{\rho}}{3} + \frac{\langle \hat{J}_x \rangle_{\rho}}{6} - \frac{i}{2} \langle [\hat{J}_z^2, \hat{J}_y^2] \rangle_{\rho}, \quad (\text{S74})$$

and

$$-i\langle[\hat{J}_x^2, \hat{J}_{yz}^2]\rangle_\rho = \frac{2\sqrt{2}(\langle\hat{J}_{zx}^3\rangle_\rho - \langle\hat{J}_{z\bar{x}}^3\rangle_\rho - \langle\hat{J}_{xy}^3\rangle_\rho - \langle\hat{J}_{x\bar{y}}^3\rangle_\rho)}{3} - \frac{i}{2}\langle[\hat{J}_x^2, \hat{J}_y^2]\rangle_\rho - \frac{i}{2}\langle[\hat{J}_x^2, \hat{J}_z^2]\rangle_\rho, \quad (\text{S75})$$

$$-i\langle[\hat{J}_y^2, \hat{J}_{zx}^2]\rangle_\rho = \frac{2\sqrt{2}(\langle\hat{J}_{xy}^3\rangle_\rho - \langle\hat{J}_{x\bar{y}}^3\rangle_\rho - \langle\hat{J}_{yz}^3\rangle_\rho - \langle\hat{J}_{y\bar{z}}^3\rangle_\rho)}{3} - \frac{i}{2}\langle[\hat{J}_y^2, \hat{J}_x^2]\rangle_\rho - \frac{i}{2}\langle[\hat{J}_y^2, \hat{J}_z^2]\rangle_\rho, \quad (\text{S76})$$

$$-i\langle[\hat{J}_z^2, \hat{J}_{xy}^2]\rangle_\rho = \frac{2\sqrt{2}(\langle\hat{J}_{yz}^3\rangle_\rho - \langle\hat{J}_{y\bar{z}}^3\rangle_\rho - \langle\hat{J}_{zx}^3\rangle_\rho - \langle\hat{J}_{z\bar{x}}^3\rangle_\rho)}{3} - \frac{i}{2}\langle[\hat{J}_z^2, \hat{J}_x^2]\rangle_\rho - \frac{i}{2}\langle[\hat{J}_z^2, \hat{J}_y^2]\rangle_\rho, \quad (\text{S77})$$

then to further obtain that

$$\begin{aligned} -i\langle[\hat{J}_{xy}^2, \hat{J}_{yz}^2]\rangle_\rho &= \frac{-i\langle[\hat{J}_x^2, \hat{J}_{yz}^2]\rangle_\rho - i\langle[\hat{J}_y^2, \hat{J}_{yz}^2]\rangle_\rho + i\langle[\hat{J}_y^2, \hat{J}_{xy}^2]\rangle_\rho + i\langle[\hat{J}_z^2, \hat{J}_{xy}^2]\rangle_\rho}{2} + \frac{i\langle[\hat{J}_x^2, \hat{J}_y^2]\rangle_\rho + i\langle[\hat{J}_x^2, \hat{J}_z^2]\rangle_\rho + i\langle[\hat{J}_y^2, \hat{J}_z^2]\rangle_\rho}{4} \\ &\quad + \text{cov}_\rho(\hat{J}_y, \hat{J}_z + \hat{J}_x) - \langle\hat{J}_y^3\rangle_\rho - \frac{\langle\hat{J}_y\rangle_\rho}{4} + \langle\hat{J}_y\rangle_\rho(\langle\hat{J}_z\rangle_\rho + \langle\hat{J}_x\rangle_\rho), \end{aligned} \quad (\text{S78})$$

$$\begin{aligned} -i\langle[\hat{J}_{xy}^2, \hat{J}_{zx}^2]\rangle_\rho &= \frac{-i\langle[\hat{J}_x^2, \hat{J}_{zx}^2]\rangle_\rho - i\langle[\hat{J}_y^2, \hat{J}_{zx}^2]\rangle_\rho + i\langle[\hat{J}_z^2, \hat{J}_{xy}^2]\rangle_\rho + i\langle[\hat{J}_x^2, \hat{J}_{xy}^2]\rangle_\rho}{2} + \frac{i\langle[\hat{J}_x^2, \hat{J}_z^2]\rangle_\rho + i\langle[\hat{J}_y^2, \hat{J}_z^2]\rangle_\rho + i\langle[\hat{J}_y^2, \hat{J}_x^2]\rangle_\rho}{4} \\ &\quad - \text{cov}_\rho(\hat{J}_x, \hat{J}_y + \hat{J}_z) + \langle\hat{J}_x^3\rangle_\rho + \frac{\langle\hat{J}_x\rangle_\rho}{4} - \langle\hat{J}_x\rangle_\rho(\langle\hat{J}_y\rangle_\rho + \langle\hat{J}_z\rangle_\rho), \end{aligned} \quad (\text{S79})$$

$$\begin{aligned} -i\langle[\hat{J}_{yz}^2, \hat{J}_{zx}^2]\rangle_\rho &= \frac{-i\langle[\hat{J}_y^2, \hat{J}_{zx}^2]\rangle_\rho - i\langle[\hat{J}_z^2, \hat{J}_{zx}^2]\rangle_\rho + i\langle[\hat{J}_x^2, \hat{J}_{yz}^2]\rangle_\rho + i\langle[\hat{J}_z^2, \hat{J}_{yz}^2]\rangle_\rho}{2} + \frac{i\langle[\hat{J}_y^2, \hat{J}_z^2]\rangle_\rho + i\langle[\hat{J}_y^2, \hat{J}_x^2]\rangle_\rho + i\langle[\hat{J}_z^2, \hat{J}_x^2]\rangle_\rho}{4} \\ &\quad + \text{cov}_\rho(\hat{J}_z, \hat{J}_x + \hat{J}_y) - \langle\hat{J}_z^3\rangle_\rho - \frac{\langle\hat{J}_z\rangle_\rho}{4} + \langle\hat{J}_z\rangle_\rho(\langle\hat{J}_x\rangle_\rho + \langle\hat{J}_y\rangle_\rho). \end{aligned} \quad (\text{S80})$$

#### D. Experimental details on measurement of squeezing parameters

In Fig. 2d of the main text, to calculate the linear spin squeezing parameter  $\xi_R^2$  at each time point  $t$ , we apply the experimental sequence shown in Fig. 1d of the main text, which is divided into four successive steps:

- (i) The state preparation realised by  $Y_{\frac{\pi}{2}}$  gates.
- (ii) The nonlinear evolution where all qubits are equally detuned.
- (iii) The rotation pulses to measure qubits at different directions.
- (iv) The final joint single-shot readout.

We performed experimental runs repetitively for about 200,000 times in total for each linear collective spin operator,  $\hat{J}_\beta$ , listed in Eqs. (S19–S23). We then divided the results into 80 groups. For each group with  $i = 1, 2, \dots, 80$  denoting the group index, we obtain the joint raw probabilities of 10 qubits

$$\mathcal{P}_\beta^{(i)} = \{P_{0\dots00}, P_{0\dots01}, P_{0\dots10}, \dots, P_{1\dots11}\}, \quad (\text{S81})$$

and then perform the readout correction on them to obtain the corrected probability,  $\tilde{\mathcal{P}}_\beta^{(i)}$ , after which the average of the observable,  $\langle\hat{J}_\beta\rangle_{\rho_t}^{(i)}$ , can be calculated for each group. Following the same process described above, we collect results for all the observables,  $\{\hat{J}_\beta\}$ , and calculate the linear Ramsey squeezing parameter,  $[\xi_R^2]^{(i)}$ , using Eq. (3) in the main text. The mean value and error bar of the  $\xi_R^2$  are estimated from these 80 groups of experimental data.

For the second-order nonlinear squeezing parameter,  $\xi_{\text{NL}}^2$ , as it requires a much larger number of experimental repetitions to become stable, which is time-consuming, we adopt a different method to estimate the error bar. From 84 groups of experimental data in total, we randomly select 40 groups of them and average these selected data (as a group labeled by  $j$ ) to calculate the second-order nonlinear squeezing parameter,  $[\xi_{\text{NL}}^2]^{(j)}$ . After repeating this process 10 times ( $j = 1, 2, \dots, 10$ ), we are able to estimate the error bar of the second-order nonlinear squeezing parameter by calculating the standard deviation of  $\{[\xi_{\text{NL}}^2]^{(1)}, [\xi_{\text{NL}}^2]^{(2)}, \dots, [\xi_{\text{NL}}^2]^{(10)}\}$ .

### III. EXTRACTION OF THE FISHER INFORMATION

#### A. Extraction of the Fisher information from the squared Hellinger distance

Given the generator,  $\hat{J}_y \equiv \sum_{j=1}^N \hat{\sigma}_j^y / 2$ , followed by an optimal angle,  $\alpha_{\text{opt}}$ , of the rotation along the  $x$ -axis to maximise the Fisher information, we imprint the phase  $\theta$  on the state as

$$\tilde{\rho}_t(\theta) = \exp(-i\hat{J}_y\theta) \exp(-i\hat{J}_x\alpha_{\text{opt}}) \rho_t \exp(i\hat{J}_x\alpha_{\text{opt}}) \exp(i\hat{J}_y\theta), \quad (\text{S82})$$

and measure each superconducting qubit by the single-shot readout measurement to obtain the probability distribution of the observable  $\hat{J}_z \equiv \sum_{j=1}^N \hat{\sigma}_j^z / 2$ . To extract the Fisher information [38], we consider the squared Hellinger distance as

$$d_{\text{H}}^2(\theta) = 1 - \mathcal{F}_{\text{C}}[\{P_z(0)\}, \{P_z(\theta)\}] = 1 - \sum_z \sqrt{P_z(0)P_z(\theta)}, \quad (\text{S83})$$

where the Bhattacharyya coefficient (classical fidelity) is written as

$$\mathcal{F}_{\text{C}}[\{P_z(0)\}, \{P_z(\theta)\}] = \sum_z \sqrt{P_z(0)P_z(\theta)}, \quad (\text{S84})$$

with  $P_z(\theta)$  being the probability distribution of the output  $z = -\frac{N}{2}, -\frac{N}{2} + 1, \dots, \frac{N}{2} - 1, \frac{N}{2}$  of the observable  $\hat{J}_z$ . For a small  $\theta \rightarrow 0$ , the Taylor expansion of the squared Hellinger distance is given as [36]

$$d_{\text{H}}^2(\theta) = \frac{F(0)}{8} \theta^2 + \mathcal{O}(\theta^3), \quad (\text{S85})$$

where the Fisher information (divided by 8) can be regarded as the square of the speed of the Hellinger distance

$$\sqrt{F(0)/8} = v_{\text{H}} \equiv \left. \frac{\partial d_{\text{H}}(\theta)}{\partial \theta} \right|_{\theta=0}. \quad (\text{S86})$$

In theory, by maximising the squared Hellinger distance over all possible positive operator-valued measures (POVMs)  $\{\hat{E}\}$ , the squared Bures distance can be obtained

$$d_{\text{B}}^2(\theta) = \max_{\{\hat{E}\}} d_{\text{H}}^2(\theta) = 1 - \mathcal{F}_{\text{Q}}[\tilde{\rho}_t(0), \tilde{\rho}_t(\theta)], \quad (\text{S87})$$

where the Bures fidelity (quantum fidelity) between two states  $\rho(0)$  and  $\rho(\theta)$  reads

$$\mathcal{F}_{\text{Q}}[\tilde{\rho}_t(0), \tilde{\rho}_t(\theta)] \equiv \text{Tr}[\sqrt{\sqrt{\tilde{\rho}_t(0)}\tilde{\rho}_t(\theta)\sqrt{\tilde{\rho}_t(0)}}]. \quad (\text{S88})$$

The Taylor expansion of the squared Bures distance for  $\theta \rightarrow 0$  is given as [39]

$$d_{\text{B}}^2(\theta) = \frac{F_{\text{Q}}[\tilde{\rho}_t(0)]}{8} \theta^2 + \mathcal{O}(\theta^3) \quad (\text{S89})$$

where the quantum Fisher information (divided by 8) can be regarded as the square of the speed of the Bures distance

$$\sqrt{F_{\text{Q}}[\tilde{\rho}_t(0)]/8} = v_{\text{B}} \equiv \left. \frac{\partial d_{\text{B}}(\theta)}{\partial \theta} \right|_{\theta=0}, \quad (\text{S90})$$

and gives an achievable upper bound for the Fisher information for the optimal choice of the POVMs

$$F_{\text{Q}}[\tilde{\rho}_t(0)] = \max_{\{\hat{E}\}} F(0). \quad (\text{S91})$$

#### B. Experimental details for extracting the Fisher information

In Fig. 4 of the main text, to obtain the Fisher information at time  $t$ , we apply the experimental sequence in Fig. 3a, which successively includes: (i) the state preparation pulse  $Y_{\frac{\pi}{2}}$ , (ii) the nonlinear evolution  $\exp(-i\hat{H}t)$ , (iii) the optimisation rotation

$X_\alpha$ , and (iv) the joint readouts in cases with and without the phase pulse  $Y_\theta$  inserted before the readouts. For each  $\theta$  and  $\alpha$ , we obtain the joint readout probabilities of 19 qubits

$$\mathcal{P}(\theta, \alpha) = \{P_{0\dots00}, P_{0\dots01}, P_{0\dots10}, \dots, P_{1\dots11}\}, \quad (\text{S92})$$

from which the probabilities  $\{P_z(\theta, \alpha)\}$  are extracted after performing the readout correction on  $\mathcal{P}(\theta, \alpha)$ . The Fisher information  $F(\theta = 0, \alpha)$  for different  $\alpha$  can then be extracted from the squared Hellinger distance of two states with and without the phase pulse  $Y_\theta$  inserted before the readouts using

$$F(0, \alpha) \simeq \frac{8 \times d_{\text{H}}^2(\theta, \alpha)}{\theta^2}, \quad (\text{S93})$$

with  $\theta$  being selected as a small value ( $-0.05$  rad in our experiment). The quadratic curve fitting of the square of the Hellinger distance versus the phase (Fig. 4a in the main text) fits the experimental data well for a relative small phase.

The optimised Fisher information is saturated by the optimal tomography angle  $\alpha_{\text{opt}}$  along the  $x$ -axis

$$F_{\text{opt}}(0) = \max_{\alpha} [F(0, \alpha)]. \quad (\text{S94})$$

To estimate the error bar, we perform about 600,000 experimental runs and obtain about 240 groups of the probabilities  $\{P_z(\theta, \alpha)\}^{(i)}$  for each  $\alpha$  and  $\theta$ , where  $i$  denotes the group index. After performing the readout correction on these probabilities, we randomly select 60 groups of them to calculate the Fisher information using the method described above. We repeat this random sampling process 10 times to calculate the final error bar of the Fisher information. Note that for  $t = 48$  ns, we only obtained 180 groups of probabilities from about 400,000 repetitive experimental runs in total, and we randomly selected 40 groups of them to calculate the error bar.

- 
- [1] C. A. Sackett, D. Kielpinski, B. E. King, C. Langer, V. Meyer, C. J. Myatt, M. Rowe, Q. A. Turchette, W. M. Itano, D. J. Wineland, and C. Monroe, Experimental entanglement of four particles, *Nature* **404**, 256 (2000).
  - [2] V. Meyer, M. A. Rowe, D. Kielpinski, C. A. Sackett, W. M. Itano, C. Monroe, and D. J. Wineland, Experimental demonstration of entanglement-enhanced rotation angle estimation using trapped ions, *Phys. Rev. Lett.* **86**, 5870 (2001).
  - [3] D. Leibfried, B. DeMarco, V. Meyer, D. Lucas, M. Barrett, J. Britton, W. M. Itano, B. Jelenković, C. Langer, T. Rosenband, and D. J. Wineland, Experimental demonstration of a robust, high-fidelity geometric two ion-qubit phase gate, *Nature* **422**, 412 (2003).
  - [4] D. Leibfried, M. D. Barrett, T. Schaetz, J. Britton, J. Chiaverini, W. M. Itano, J. D. Jost, C. Langer, and D. J. Wineland, Toward Heisenberg-limited spectroscopy with multiparticle entangled states, *Science* **304**, 1476 (2004).
  - [5] D. Leibfried, E. Knill, S. Seidelin, J. Britton, R. B. Blakestad, J. Chiaverini, D. B. Hume, W. M. Itano, J. D. Jost, C. Langer, R. Ozeri, R. Reichle, and D. J. Wineland, Creation of a six-atom ‘Schrödinger cat’ state, *Nature* **438**, 639 (2005).
  - [6] J. Estève, C. Gross, A. Weller, S. Giovanazzi, and M. K. Oberthaler, Squeezing and entanglement in a Bose–Einstein condensate, *Nature* **455**, 1216 (2008).
  - [7] J. Appel, P. J. Windpassinger, D. Oblak, U. B. Hoff, N. Kjærgaard, and E. S. Polzik, Mesoscopic atomic entanglement for precision measurements beyond the standard quantum limit, *PNAS* **106**, 10960 (2009).
  - [8] I. D. Leroux, M. H. Schleier-Smith, and V. Vuletić, Implementation of cavity squeezing of a collective atomic spin, *Phys. Rev. Lett.* **104**, 073602 (2010).
  - [9] M. H. Schleier-Smith, I. D. Leroux, and V. Vuletić, States of an ensemble of two-level atoms with reduced quantum uncertainty, *Phys. Rev. Lett.* **104**, 073604 (2010).
  - [10] C. Gross, T. Zibold, E. Nicklas, J. Estève, and M. K. Oberthaler, Nonlinear atom interferometer surpasses classical precision limit, *Nature* **464**, 1165 (2010).
  - [11] M. F. Riedel, P. Böhi, Y. Li, T. W. Hänsch, A. Sinatra, and P. Treutlein, Atom-chip-based generation of entanglement for quantum metrology, *Nature* **464**, 1170 (2010).
  - [12] I. D. Leroux, M. H. Schleier-Smith, and V. Vuletić, Orientation-dependent entanglement lifetime in a squeezed atomic clock, *Phys. Rev. Lett.* **104**, 250801 (2010).
  - [13] A. Louchet-Chauvet, J. Appel, J. J. Renema, D. Oblak, N. Kjaergaard, and E. S. Polzik, Entanglement-assisted atomic clock beyond the projection noise limit, *New J. Phys.* **12**, 065032 (2010).
  - [14] Z. L. Chen, J. G. Bohnet, S. R. Sankar, J. Y. Dai, and J. K. Thompson, Conditional spin squeezing of a large ensemble via the vacuum rabi splitting, *Phys. Rev. Lett.* **106**, 133601 (2011).
  - [15] T. Monz, P. Schindler, J. T. Barreiro, M. Chwalla, D. Nigg, W. A. Coish, M. Harlander, W. Hänsel, M. Hennrich, and R. Blatt, 14-qubit entanglement: Creation and coherence, *Phys. Rev. Lett.* **106**, 130506 (2011).
  - [16] B. Lücke, M. Scherer, J. Kruse, L. Pezzé, F. Deuretzbacher, P. Hyllus, O. Topic, J. Peise, W. Ertmer, J. Arlt, L. Santos, A. Smerzi, and C. Klempt, Twin matter waves for interferometry beyond the classical limit, *Science* **334**, 773 (2011).
  - [17] C. D. Hamley, C. S. Gerving, T. M. Hoang, E. M. Bookjans, and M. S. Chapman, Spin-nematic squeezed vacuum in a quantum gas, *Nat. Phys.* **8**, 305 (2012).



- [18] R. J. Sewell, M. Koschorreck, M. Napolitano, B. Dubost, N. Behbood, and M. W. Mitchell, Magnetic sensitivity beyond the projection noise limit by spin squeezing, *Phys. Rev. Lett.* **109**, 253605 (2012).
- [19] T. Berrada, S. van Frank, R. Bücker, T. Schumm, J.-F. Schaff, and J. Schmiedmayer, Integrated Mach-Zehnder interferometer for Bose-Einstein condensates, *Nat. Commun.* **4**, 2077 (2013).
- [20] C. F. Ockeloen, R. Schmied, M. F. Riedel, and P. Treutlein, Quantum metrology with a scanning probe atom interferometer, *Phys. Rev. Lett.* **111**, 143001 (2013).
- [21] R. J. Sewell, M. Napolitano, N. Behbood, G. Colangelo, F. Martin Ciurana, and M. W. Mitchell, Ultrasensitive atomic spin measurements with a nonlinear interferometer, *Phys. Rev. X* **4**, 021045 (2014).
- [22] H. Strobel, W. Muessel, D. Linnemann, T. Zibold, D. B. Hume, L. Pezzè, A. Smerzi, and M. K. Oberthaler, Fisher information and entanglement of non-Gaussian spin states, *Science* **345**, 424 (2014).
- [23] J. G. Bohnet, K. C. Cox, M. A. Norcia, J. M. Weiner, Z. Chen, and J. K. Thompson, Reduced spin measurement back-action for a phase sensitivity ten times beyond the standard quantum limit, *Nat. Photon.* **8**, 731 (2014).
- [24] W. Muessel, H. Strobel, D. Linnemann, D. B. Hume, and M. K. Oberthaler, Scalable spin squeezing for quantum-enhanced magnetometry with Bose-Einstein condensates, *Phys. Rev. Lett.* **113**, 103004 (2014).
- [25] W. Muessel, H. Strobel, D. Linnemann, T. Zibold, B. Juliá-Díaz, and M. K. Oberthaler, Twist-and-turn spin squeezing in Bose-Einstein condensates, *Phys. Rev. A* **92**, 023603 (2015).
- [26] G. Barontini, L. Hohmann, F. Haas, J. Estève, and J. Reichel, Deterministic generation of multiparticle entanglement by quantum Zeno dynamics, *Science* **349**, 1317 (2015).
- [27] O. Hosten, N. J. Engelsen, R. Krishnakumar, and M. A. Kasevich, Measurement noise 100 times lower than the quantum-projection limit using entangled atoms, *Nature* **529**, 505 (2016).
- [28] K. C. Cox, G. P. Greve, J. M. Weiner, and J. K. Thompson, Deterministic squeezed states with collective measurements and feedback, *Phys. Rev. Lett.* **116**, 093602 (2016).
- [29] J. G. Bohnet, B. C. Sawyer, J. W. Britton, M. L. Wall, A. M. Rey, M. Foss-Feig, and J. J. Bollinger, Quantum spin dynamics and entanglement generation with hundreds of trapped ions, *Science* **352**, 1297 (2016).
- [30] I. Kruse, K. Lange, J. Peise, B. Lücke, L. Pezzè, J. Arlt, W. Ertmer, C. Lisdat, L. Santos, A. Smerzi, and C. Klempt, Improvement of an atomic clock using squeezed vacuum, *Phys. Rev. Lett.* **117**, 143004 (2016).
- [31] Y.-Q. Zou, L.-N. Wu, Q. Liu, X.-Y. Luo, S.-F. Guo, J.-H. Cao, M. K. Tey, and L. You, Beating the classical precision limit with spin-1 Dicke states of more than 10,000 atoms, *PNAS* **115**, 6381 (2018).
- [32] A. Omran, H. Levine, A. Keesling, G. Semeghini, T. T. Wang, S. Ebadi, H. Bernien, A. S. Zibrov, H. Pichler, S. Choi, J. Cui, M. Rossignolo, P. Rembold, S. Montangero, T. Calarco, M. Endres, M. Greiner, V. Vuletić, and M. D. Lukin, Generation and manipulation of Schrödinger cat states in Rydberg atom arrays, *Science* **365**, 570 (2019).
- [33] C. Song, K. Xu, H. K. Li, Y.-R. Zhang, X. Zhang, W. X. Liu, Q. J. Guo, Z. Wang, W. H. Ren, J. Hao, H. Feng, H. Fan, D. N. Zheng, D.-W. Wang, H. Wang, and S.-Y. Zhu, Generation of multicomponent atomic Schrödinger cat states of up to 20 qubits, *Science* **365**, 574 (2019).
- [34] R. Krischek, C. Schwemmer, W. Wiczkorek, H. Weinfurter, P. Hyllus, L. Pezzè, and A. Smerzi, Useful multiparticle entanglement and sub-shot-noise sensitivity in experimental phase estimation, *Phys. Rev. Lett.* **107**, 080504 (2011).
- [35] L.-Z. Liu, Y.-Z. Zhang, Z.-D. Li, R. Zhang, X.-F. Yin, Y.-Y. Fei, L. Li, N.-L. Liu, F. Xu, Y.-A. Chen, and J.-W. Pan, Distributed quantum phase estimation with entangled photons, *Nat. Photon.* **15**, 137 (2021).
- [36] L. Pezzè, A. Smerzi, M. K. Oberthaler, R. Schmied, and P. Treutlein, Quantum metrology with nonclassical states of atomic ensembles, *Rev. Mod. Phys.* **90**, 035005 (2018).
- [37] M. Gessner, A. Smerzi, and L. Pezzè, Metrological nonlinear squeezing parameter, *Phys. Rev. Lett.* **122**, 090503 (2019).
- [38] W. Zhong, Z. Sun, J. Ma, X. Wang, and F. Nori, Fisher information under decoherence in Bloch representation, *Phys. Rev. A* **87**, 022337 (2013).
- [39] S. L. Braunstein and C. M. Caves, Statistical distance and the geometry of quantum states, *Phys. Rev. Lett.* **72**, 3439 (1994).